bioRxiv preprint doi: https://doi.org/10.1101/2021.05.27.443845; this version posted May 29, 2021. The copyright holder for this preprint (which was not certified by peer review) is the author/funder. All rights reserved. No reuse allowed without permission.

1 **Title**

2 **RSL24D1 sustains steady-state ribosome biogenesis and pluripotency**
3 **translational programs in embryonic stem cells.**

4

5 **Authors**

6 Sébastien Durand[1,2*], Marion Bruelle[1,2*], Fleur Bourdelais[1,2,3*], Bigitha Bennychen[4],
7 Juliana Blin-Gonthier[5], Caroline Isaac[1,2], Aurélia Huyghe[2,6], Antoine Seyve[1,2], Christophe
8 Vanbelle[2], David Meyronet[1,2,7], Frédéric Catez[2,8], Jean-Jacques Diaz[2,8], Fabrice Lavial[2,6],
9 Emiliano P. Ricci[5], François Ducray[1,2], Mathieu Gabut[1,2,+].

10

11 **Affiliations**

12 1. Stemness in gliomas laboratory, Cancer Initiation and Tumoral Cell Identity (CITI)
13 Department.
14 2. Cancer Research Centre of Lyon (CRCL) INSERM 1052, CNRS 5286, Université Claude
15 Bernard Lyon I, Centre Léon Bérard, 69008 Lyon, France.
16 3. Inovarion, 75005 Paris, France.
17 4. University of Ottawa, Dept. of Biochemistry, Microbiology and Immunology. National
18 Research Council Canada, Human Health Therapeutics Research Centre, Ottawa,
19 Canada.
20 5. Laboratoire de Biologie et de Modélisation de la Cellule, ENS de Lyon, CNRS UMR
21 5239, Inserm U1293, Lyon, France.
22 6. Cellular reprogramming, stem cells and oncogenesis, Equipe labellisée la Ligue contre
23 le cancer, Labex Dev2Can, CITI Department.
24 7. Institut de Pathologie Est, Hospices Civils de Lyon, 69002 Lyon, France.
25 8. Ribosomes, translation and cancer laboratory, CITI Department.

26

27 * Authors contributed equally to this work.
28 + Author for correspondence (mathieu.gabut@inserm.fr)

bioRxiv preprint doi: https://doi.org/10.1101/2021.05.27.443845; this version posted May 29, 2021. The copyright holder for this preprint (which was not certified by peer review) is the author/funder. All rights reserved. No reuse allowed without permission.

29 **Abstract**
30 Embryonic stem cell (ESC) fate decisions are regulated by a complex molecular circuitry
31 that requires tight and coordinated gene expression regulations at multiple levels from
32 chromatin organization to mRNA processing. Recently, ribosome biogenesis and
33 translation have emerged as key regulatory pathways that efficiently control stem cell
34 homeostasis. However, the molecular mechanisms underlying the regulation of these
35 pathways remain largely unknown to date. Here, we analyzed the expression, in mouse
36 ESCs, of over 300 genes involved in ribosome biogenesis and we identified RSL24D1 as
37 the most differentially expressed between self-renewing and differentiated ESCs.
38 RSL24D1 is highly expressed in multiple mouse pluripotent stem cell models and its
39 expression profile is conserved in human ESCs. RSL24D1 is associated with nuclear pre-
40 ribosomes and is required for the maturation and the synthesis of 60S subunits in
41 mouse ESCs. Interestingly, RSL24D1 depletion significantly impairs global translation,
42 particularly of key pluripotency factors, including POU5F1 and NANOG, as well as
43 components of the polycomb repressive complex 2 (PRC2). Consistently, RSL24D1 is
44 required for mouse ESC self-renewal and proliferation. Taken together, we show that
45 RSL24D1-dependant ribosome biogenesis is required to both sustain the expression of
46 pluripotent transcriptional programs and silence developmental programs, which
47 concertedly dictate ESC homeostasis.
48

49 **Introduction**
50 Pluripotent stem cells (PSCs), including embryonic stem cells (ESCs) and induced
51 pluripotent stem cells (iPSCs), have the unique abilities to self-renew in a naive state
52 while remaining competent to differentiate into a spectrum of lineages that compose
53 developing embryonic tissues. This ambivalent state is tightly and dynamically
54 coordinated at different steps of gene expression, which have been extensively
55 described at the chromatin (1), transcriptional (2, 3) and post-transcriptional levels (4-
56 6). This led to the identification of key regulatory epigenetic and transcriptional
57 programs that rapidly rewire gene expression and regulate complex cell fate transitions
58 in response to environmental cues (1, 3, 7, 8). For instance, chromatin modifications
59 mediated by the Polycomb Repressive Complexes 1 and 2 (PRC1 and PRC2) have been
60 shown to play pivotal roles in the transcriptional regulation of pluripotency and
61 differentiation of PSCs (1, 7-9). However, multiple studies suggest that, in many

bioRxiv preprint doi: https://doi.org/10.1101/2021.05.27.443845; this version posted May 29, 2021. The copyright holder for this preprint (which was not certified by peer review) is the author/funder. All rights reserved. No reuse allowed without permission.

62 circumstances, messenger RNA (mRNA) and protein levels are poorly correlated,
63 including in ESCs and iPSCs, therefore highlighting the importance of translational
64 regulations for shaping the cellular proteome landscape required for cell fate changes
65 (10-15). The relevance of such observations is strengthened by recent studies
66 highlighting that translation is regulated during PSCs differentiation, with a lower
67 translation efficiency in undifferentiated ESCs, but also in adult stem cell models
68 compared to differentiated progenies (16-19). Remarkably, murine ESC proliferation is
69 regulated by interdependent layers involving translation, euchromatin organization and
70 transcriptional control (20). This is well illustrated by HTATSF1-dependent
71 coordination of protein synthesis with ribosomal RNA (rRNA) processing during human
72 ESC differentiation (21). Taken together, this compelling evidence therefore
73 demonstrates that the regulation of protein synthesis plays a key role in defining stem
74 cell fate.
75 In eukaryotes, ribosome biogenesis is a complex and multistep process that involves
76 different cellular compartments, consecutively the nucleoli, the nucleoplasm and the
77 cytoplasm, as well as over 280 ribosome biogenesis factors (RBFs) and different families
78 of non-coding RNAs (22-24). Many studies have established that ribosome biogenesis is
79 finely regulated in stem cells and may directly control stem cell properties (16). First,
80 despite having a low protein synthesis activity, ESCs display higher levels of rRNA
81 transcription rates compared to endodermal-lineage committed cells (25). Moreover,
82 the nuclear remodelling complex NoRC has been shown to coordinate rRNA
83 transcription and proliferation rates in mouse ESCs (26). Similarly, several RFBs are
84 expressed at higher levels in ESCs compared to differentiated progenies (27), including
85 Nucleolin (28), Dyskerin Pseudouridine Synthase 1 (DKC1) (29) and Fibrillarin (FBL)
86 (30), and are required for ESC self-renewal. In addition to these well-described essential
87 RBFs controlling rRNA expression and post-transcriptional modifications, it appears
88 that ribosome subunit-specific RBFs are required to support ESC maintenance. Indeed,
89 several factors implicated in the maturation of the 40S small ribosome subunit (SSU) are
90 preferentially expressed in naive ESCs compared to differentiated progenies and
91 support the translation of key pluripotency transcription factors (PTFs) such as NANOG
92 (31). Notably, Notchless, a RBF of the 60S large ribosome subunit (LSU), is required for
93 the Inner Cell Mass survival during early mouse embryogenesis, yet it is unclear
94 whether ribosome biogenesis is implicated in this context, in contrast to Notchless

bioRxiv preprint doi: https://doi.org/10.1101/2021.05.27.443845; this version posted May 29, 2021. The copyright holder for this preprint (which was not certified by peer review) is the author/funder. All rights reserved. No reuse allowed without permission.

95 functions in adult stem cells homeostasis (32-35). Thus, to date, the contributions of
96 ribosome subunit-specific RBFs, especially of pre-60S RBFs, to the steady-state
97 stoichiometry of the 40S and 60S subunits and their impact on the regulation of PSC fate
98 decision remain unclear and should be further investigated.
99 Here, we show that RSL24D1, a conserved homolog of the yeast pre-60S maturation and
100 export factor Rlp24, is expressed at high levels in mouse and human PSCs compared to
101 differentiated progenies. We demonstrate that RSL24D1 is essential for the maturation
102 of the LSU in pluripotent mouse ESCs. RSL24D1 is also required to maintain a steady-
103 state level of translation, in particular of PTFs, such as NANOG and POU5F1 that control
104 pluripotent transcriptional programs, but also of PRC2 factors that maintain repressive
105 H3K27me3 marks over developmental and differentiation genes to prevent their
106 premature activation. Moreover, high levels of RSL24D1 are required to support mouse
107 ESC proliferation and self-renewal. Altogether, these results establish for the first time
108 that a *bona fide* 60S biogenesis and the resulting proper translation status are
109 coordinated with transcription and chromatin regulation networks to control ESC
110 homeostasis.
111
112 **Results**
113 _Rsl24d1 expression is enriched in murine and human pluripotent cells._
114 To identify factors contributing to ribosome assembly in pluripotent stem cells, we first
115 defined the mRNA expression profiles of 303 genes, including RBFs and ribosomal
116 proteins (RPs), in murine iPSC clones, ESCs and differentiated cell lines using publicly
117 available RNA-seq data (36) (Supplemental Fig. S1A and Table 1). The majority (70%) of
118 factors associated with the biogenesis of the LSU and SSU, as well as RPs were expressed
119 at higher levels in pluripotent cells compared to differentiated cells (fold change >1,5)
120 (Fig. 1A). Among these factors, we identified Rsl24d1, a predicted ribosome biogenesis
121 protein, which displayed the most striking expression change between differentiated
122 mouse cell lines and PSCs (Log2 fold change > 13,3) (Fig. 1A). We next confirmed that
123 RSL24D1 was also expressed at a higher level in mouse pluripotent CGR8 ESCs cultured
124 either in serum+LIF (ESC^{FBS}) or in 2i-induced naïve ground state (ESC^{2i}) conditions
125 compared to *in vitro* ESC-derived 12-day old differentiated embryoid bodies (EBs)
126 containing beating cardiomyocytes (EB^{12}) (Fig. 1B). In contrast, the expression of RPL8,

bioRxiv preprint doi: https://doi.org/10.1101/2021.05.27.443845; this version posted May 29, 2021. The copyright holder for this preprint (which was not certified by peer review) is the author/funder. All rights reserved. No reuse allowed without permission.

127 a canonical RP of the LSU, remained globally unchanged at the protein level as ESCs
128 differentiate into EBs (Fig. 1B).
129 To get more insights into the regulation of Rsl24d1 expression in PSCs, we next assessed
130 the dynamics of Rsl24d1 expression during the kinetics of ESC-derived EB
131 differentiation. RT-qPCR assays confirmed that the expression of pluripotency
132 transcription factors Pou5f1, Klf4, Nanog and Sox2 rapidly decreased upon ESC
133 differentiation into EBs (Supplemental Fig. S1B). Interestingly, Rsl24d1 is expressed at
134 the highest level in mouse CGR8 ESCs and is progressively downregulated after
135 differentiation initiation to reach its lowest expression level in EB^{12}, thereby correlating
136 with the expression profiles of key PTFs. Consistent with mRNA levels, RSL24D1 protein
137 expression was strongly lowered after 5 days of EB formation and further decreased as
138 the differentiation proceeded to reach a minimal expression in EB^{12} (Supplemental Fig.
139 S1C). The expression of additional RPs also decreased, yet to a lower extent than
140 RSL24D1, while the downregulation of two biogenesis factors, EIF6 and NOG1, rather
141 followed RSL24D1's profile. In addition, we assessed the expression of RSL24D1 in two
142 additional mouse ESCs lines (R1 and G4) cultured in similar conditions (ESC^{2i}, ESC^{FBS},
143 EB^{12}) (Fig. 1C). Although RSL24D1 was expressed at different basal levels in the three
144 ESC models, these results confirmed that RSL24D1 levels were significantly higher in
145 ESCs maintained in pluripotent states than in ESC-derived differentiated EBs.
146 Altogether, these results convincingly demonstrate that RSL24D1 expression is high in
147 murine ESCs and strongly decreases upon differentiation.
148 We then hypothesized that the expression of Rsl24d1 would rather be determined by
149 the pluripotency status than by the embryonic origin. Therefore, pluripotent cells from
150 non-embryonic origin should also express high levels of RSL24D1 compared to their
151 differentiated counterparts. To evaluate this hypothesis, iPSCs were generated after
152 somatic reprogramming of mouse embryonic fibroblasts (MEFs) by forced expression of
153 Pou5f1, Klf4, c-Myc and Sox2 (OKMS) (37). The kinetics of somatic reprogramming was
154 assessed by the activation of both endogenous Pou5f1 and Nanog mRNAs (Supplemental
155 Fig. S1D). While RPL8 expression remained globally unchanged, RSL24D1 expression
156 was highly increased in 14-day old iPSCs compared to parental MEFs (Fig. 1D). Since
157 early steps of iPSC formation are highly heterogeneous and stochastic (38, 39), we next
158 investigated Rsl24d1 expression in cells with enhanced reprogramming potential at the
159 single cell level from published data (40). Interestingly, single-cell RNA-seq data and fate

bioRxiv preprint doi: https://doi.org/10.1101/2021.05.27.443845; this version posted May 29, 2021. The copyright holder for this preprint (which was not certified by peer review) is the author/funder. All rights reserved. No reuse allowed without permission.

160 trajectory detection by Guo and colleagues revealed that Rsl24d1 expression was
161 strongly enhanced in a continuum of cells representing different stages of active
162 reprogramming (pre-PCs) compared to cells that are engaged in earlier steps of the
163 reprogramming path (RP) (Supplemental Fig. S1E). Strikingly, Rsl24d1 levels were even
164 further increased in chimera-competent reprogrammed cells (PCs) expressing high
165 levels of pluripotency factors including Nanog and Esrrb (Supplemental Fig. S1E).
166 Altogether, these observations suggest that Rsl24d1 expression is significantly enriched
167 in mouse PSCs regardless of their embryonic origins.
168 We next investigated whether the regulation of Rsl24d1 expression was evolutionarily
169 conserved in human PSCs. RNA-seq analysis indicated that, similarly to their murine
170 counterparts, human PSCs expressed higher levels of *RSL24D1* mRNAs compared to
171 differentiated cell lines or tissues (Fig. 1E) (36). Interestingly, western blot analyses of
172 RSL24D1 in human OSCAR ESCs cultured in FGF2-supplemented self-renewal media and
173 in ESC-derived EBs ("Diff.") revealed a marked decrease of RSL24D1 upon
174 differentiation (Fig. 1F) (41). In addition, RSL24D1 was expressed at similar levels in
175 both human OSCAR and H9 ESCs maintained either in primed (TL and FGF2) or naive-
176 like (TL2i) conditions (41) (Supplemental Fig. S1F), whereas RSL24D1 expression was
177 rather low in adult human tissues compared to human ESCs (Supplemental Fig. S1G).
178 Taken together, these results indicate that Rsl24d1 expression is high in PSCs and
179 decreases upon loss of pluripotency, and that this regulation is evolutionarily conserved.
180

181 *RSL24D1 is a biogenesis factor associated with nuclear pre-ribosomes in mouse ESCs*

182 The role of RSL24D1 in higher eukaryotes remains unknown, therefore, to gain insight
183 into its molecular functions in mouse ESCs, we first compared its sequence and structure
184 with conserved homologs. Indeed, Rlp24, the yeast homolog of RSL24D1, is a ribosome
185 biogenesis factor involved in the export of nuclear pre-60S ribosomal particles from the
186 nucleus to the cytoplasm where they undergo the final steps of maturation, including
187 Rlp24 substitution by the canonical ribosomal protein Rpl24 (23, 42). Multiple protein
188 alignments of yeast Rlp24 to higher eukaryote homologs, including murine and human
189 RSL24D1, revealed that the first 130 amino acids of Rlp24 were well conserved from
190 yeast to human (Supplemental Fig. S2A, B). In particular, RSL24D1 homologs were
191 strongly conserved in mammals, with a sequence identity over 96%, but lacked the
192 yeast-specific C-terminal extension of Rlp24.

bioRxiv preprint doi: https://doi.org/10.1101/2021.05.27.443845; this version posted May 29, 2021. The copyright holder for this preprint (which was not certified by peer review) is the author/funder. All rights reserved. No reuse allowed without permission.

193 To further assess the degree of conservation between higher eukaryote RSL24D1 and its
194 yeast homolog, we next compared the structure of mouse RSL24D1 with cryo-EM
195 structures of yeast and human protein homologs, which have been recently obtained
196 from nuclear pre-60S intermediates (Fig. 2A) (43-46). Similarly to yeast, cryo-EM
197 structures of human pre-60S particles revealed the presence of RSL24D1 in
198 nucleoplasmic stages of pre-60S assembly (states pre-A and A) while it was absent from
199 later cytoplasmic stages of pre-60S maturation (46). As the N-terminal region of Rlp24
200 homologs was the most conserved during evolution, we used these cryo-EM structures
201 to model the structure of the mouse RSL24D1 N-terminus from its amino acid sequence.
202 Interestingly, structure alignments indicate that the predicted structure of the first 135
203 amino acids of mouse RSL24D1 almost perfectly matches the yeast Rlp24 and human
204 RSL24D1 structures from nuclear pre-60S intermediates (Fig. 2A) (46). Altogether,
205 these results strongly support a conserved function of RSL24D1 in the nuclear
206 maturation of the pre-60S particles in mouse ESCs.
207 To test this hypothesis, we next analyzed the localization of RSL24D1 in mouse CGR8
208 ESCs. Since no difference in RSL24D1 expression was observed between the ESC^{2i} and
209 ESC^{FBS} conditions, all following experiments were performed with CGR8 cells cultured in
210 media containing serum and LIF (ESC^{FBS}). In these conditions, RSL24D1 was expressed
211 in all colony-forming ESCs regardless of POU5F1 steady-state levels (Supplemental Fig.
212 S2C) and was predominantly concentrated within nuclear foci containing FBL (Fig. 2B),
213 therefore suggesting that RSL24D1 is mostly located in ESC nucleoli (47).
214 We then asked whether RSL24D1 was associated with pre-ribosomal particles in mouse
215 ESC^{FBS} colonies. Following cell fractionation, pre-ribosomal and ribosomal particles
216 were respectively isolated from nuclear and cytoplasmic fractions by ultracentrifugation
217 on sucrose cushions. In contrast to RPL8 and RPS6 that are both present in nuclear pre-
218 ribosomes and in cytoplasmic ribosomes, RPL24 is exclusively present in cytoplasmic
219 ribosomes (Fig. 2C). This is consistent with observations that Rpl24 replaces Rlp24 in
220 pre-60S particles after nuclear export in yeast and human (23, 42, 46). In addition, the
221 LSU biogenesis factor EIF6, homolog of yeast Tif6, co-purifies with both nuclear and
222 cytoplasmic ribosomal particles, whereas RSL24D1 is predominantly detected in nuclear
223 pre-ribosomes (Fig. 2C). Cell fractionation assays confirmed that RSL24D1 is
224 predominantly detected in the nuclear fraction (68%) and to a lower extent in the
225 cytoplasmic fraction (32%), while RPL24 is almost exclusively present in the cytoplasm

bioRxiv preprint doi: https://doi.org/10.1101/2021.05.27.443845; this version posted May 29, 2021. The copyright holder for this preprint (which was not certified by peer review) is the author/funder. All rights reserved. No reuse allowed without permission.

226 (95%) (Supplemental Fig. S2D). RSL24D1 is also slightly associated with cytoplasmic
227 ribosomes yet to a lower extent compared to EIF6, suggesting that RSL24D1 is rapidly
228 removed from cytoplasmic pre-ribosomes and most likely replaced by RPL24 after
229 nuclear export. To confirm that RSL24D1 is associated with pre-60S particles,
230 cytoplasmic fractions were analyzed by polysome profiling assays to separate the 40S
231 (SSU), 60S (LSU), 80S (monosomes) and polysomes (Supplemental Fig. S2E). As
232 expected, RPL8 and RPS6 are predominantly detected in 60S and 40S ribosomal
233 fractions, respectively, and both proteins are also present in 80S monosomes and
234 polysomes (Fig. 2D). In contrast, RSL24D1 and EIF6 are mainly detected in 60S fractions
235 (lane 4). RSL24D1 and EIF6 are also found at a lower extent in fractions enriched in
236 monosomes (lanes 5 and 6), most likely due to an incomplete separation of 80S fractions
237 from 60S fractions, while they are not significantly detected in the 40S fractions (lane 3).
238 Altogether, these results suggest for the first time that RSL24D1 is a ribosome
239 biogenesis factor in higher eukaryotes, which is incorporated into nucleolar pre-60S
240 particles, transits to the cytoplasm and is subsequently removed from cytoplasmic pre-
241 60S.
242
243 *RSL24D1 depletion impairs both ribosome biogenesis and translation*
244 To confirm that RSL24D1 is involved in ribosome biogenesis, we then determined
245 whether its depletion impacts the accumulation and activity of mature cytoplasmic
246 ribosomes. Rsl24d1 siRNA treatment for 72 hours resulted in an efficient depletion of
247 RSL24D1 (> 67%) in mouse ESCs compared to control non-targeting siRNAs (Fig. 3A and
248 Supplemental Fig. 3A). Interestingly, RSL24D1 depletion did not detectably affect the
249 structure and the number of FBL-containing nucleoli (data not shown), therefore
250 suggesting that decreasing RSL24D1 levels did not induce major disruptions of early
251 ribosome biogenesis (48).
252 Next, the effect of RSL24D1 depletion on ribosome production was assessed by
253 polysome profiling assays conducted on control- or Rsl24d1-siRNA treated ESCs. The
254 transient depletion of RSL24D1 significantly imbalanced the accumulation of 40S, 60S
255 and 80S particles (Fig. 3B), notably causing a major loss of 60S and 80S relative to 40S
256 subunits (Fig. 3C). To achieve a more efficient and stable depletion of RSL24D1, we
257 designed two independent shRNAs targeting Rsl24d1 mRNAs (sh-Rsl24d1-1 and sh-
258 Rsl24d1-2), which resulted in a 51% and 93% depletion of RSL24D1, respectively,

bioRxiv preprint doi: https://doi.org/10.1101/2021.05.27.443845; this version posted May 29, 2021. The copyright holder for this preprint (which was not certified by peer review) is the author/funder. All rights reserved. No reuse allowed without permission.

259 compared to control shRNAs (Supplemental Fig. S3B). Interestingly, expression of sh-
260 Rsl24d1-2, which provided the most robust silencing of RSL24D1, also caused an
261 impaired accumulation of the 80S and 60S subunits, to a similar extent than siRNA-
262 treated cells (Supplemental Fig. S3C and S3D).
263 In order to further characterize molecular alterations resulting from RSL24D1
264 depletions, nuclear and cytoplasmic ribosomal fractions were isolated from ESCs treated
265 with control- and Rsl24d1-targetting siRNAs (Fig. 3D). The depletion of RSL24D1
266 resulted in a significant loss of RSL24D1 and EIF6 association to nuclear pre-ribosomes
267 (lanes 3-4) and to cytoplasmic particles (lanes 7-8). RPL24 inclusion into the
268 cytoplasmic ribosomal particles was also strongly impaired upon RSL24D1 knockdown
269 (lanes 7-8), while the presence of the canonical RPL8 in both nuclear pre-ribosomes and
270 cytoplasmic ribosomes was not significantly affected (lanes 1-8). Moreover, we
271 observed a consistent decrease of RPL24 and EIF6 expression upon RSL24D1 depletion
272 in total cytoplasmic (lanes 5-6) and nuclear (lanes 1-2) fractions, respectively. Western
273 blot assays on total extracts confirmed that RPL24 and EIF6 expression levels decreased
274 upon RSL24D1 knockdown (Fig. 3E). These observations suggest that defects in EIF6
275 and RPL24 association with pre-60S particles might interfere with the stability of these
276 proteins. Altogether, these results indicate that RSL24D1 is required for the *bona fide*
277 maturation of pre-60S particles, at least by allowing EIF6 association to nuclear pre-
278 ribosomes and RPL24 recruitment to mature cytoplasmic ribosomes. Hence, RSL24D1
279 plays a critical role in the production of mature 60S in mouse ESCs.
280 Finally, as RSL24D1 depletion impacts the LSU production, we hypothesized that
281 RSL24D1 knockdown may affect global protein synthesis in ESCs. ^{35}S pulse-chase
282 labelling assays were performed on CGR8 cells transfected with si-CTL or si-Rsl24d1, in
283 the presence or absence of cycloheximide (CHX), an inhibitor of translation elongation
284 (Fig. 3F). As expected, CHX significantly prevented the incorporation of both ^{35}S -labeled
285 methionine and cysteine in newly synthetized proteins (lanes 3-4). Strikingly, RSL24D1
286 depletion caused a significant reduction (43%) of *de novo* protein synthesis in ESCs
287 (lanes 5-6), therefore demonstrating that RSL24D1 loss decreases the global protein
288 synthesis activity of ESCs. Altogether, these results strongly suggest that RSL24D1 is as
289 an essential ribosome biogenesis factor of the LSU, which is required for the steady-state
290 protein synthesis in pluripotent ESCs.
291

bioRxiv preprint doi: https://doi.org/10.1101/2021.05.27.443845; this version posted May 29, 2021. The copyright holder for this preprint (which was not certified by peer review) is the author/funder. All rights reserved. No reuse allowed without permission.

292 *Rsl24d1 is required to maintain pluripotent transcriptional programs*

293 We next hypothesized that the effects of Rsl24d1 knockdown on ribosome biogenesis
294 and translation could impair the regulation of specific gene programs in mouse ESCs. To
295 address this question, control- or Rsl24d1-targeting siRNAs were transfected in CGR8
296 ESCs followed by RNA-Seq profiling. The top 15% of genes with the most significant
297 expression changes (>1.8 fold change; $p < 0.01$) were further analyzed. Rsl24d1 loss
298 resulted in the altered expression of 529 genes, including 250 genes upregulated (47%)
299 and 279 genes downregulated (53%) (Table 2). An analysis of Gene Ontology terms
300 associated with genes decreased upon Rsl24d1 depletion revealed a significant
301 enrichment in terms associated to immune response, metabolic processes and
302 transporter activity ($p < 0.01$) (Fig. 4A, right panel; Supplemental Fig. 4A; Tables 3A and
303 3B for a full analysis). Conversely, genes upregulated upon si-Rsl24d1 treatments are
304 strongly enriched in terms associated with developmental processes, cell differentiation,
305 cell proliferation and transcription regulation ($p < 1E-06$) (Fig. 4A, left panel;
306 Supplemental Fig. S4A; Tables 3C and 3D for a full analysis). These results suggest that
307 Rsl24d1 expression in mouse pluripotent ESCs is required to maintain a coordinated
308 regulation of specific transcription programs, including differentiation and development
309 processes, which are most likely important for the control of ESC homeostasis.

310 PSCs properties are tightly controlled by distinct epigenetic and transcriptional
311 regulators supporting the expression of programs required for self-renewal and
312 pluripotency while maintaining differentiation programs in a poised state (49, 50). Thus,
313 we hypothesized that the alteration of specific genetic programs upon Rsl24d1
314 depletion could result from the impaired expression of one or more of these key
315 transcriptional or epigenetic stemness regulators. To test this hypothesis, we first used
316 the StemChecker algorithm to identify ESC-master regulators whose expression is
317 altered upon Rsl24d1 loss (51). Interestingly, this analysis revealed that genes
318 downregulated (n=279) upon Rsl24d1 knockdown were enriched in targets of key PTFs,
319 including Nanog, Pou5f1, Smad4 and Sox2 (Fig. 4B; Table 4A for a full analysis).
320 Conversely, upregulated genes (n=250) were preferentially enriched in targets of
321 essential epigenetic regulators from the polycomb repressive complexes, including
322 Suz12, Eed and Ezh2 from PRC2, and Rnf2 from PRC1 (Fig. 4B; Table 4B for a full
323 analysis).

bioRxiv preprint doi: https://doi.org/10.1101/2021.05.27.443845; this version posted May 29, 2021. The copyright holder for this preprint (which was not certified by peer review) is the author/funder. All rights reserved. No reuse allowed without permission.

324 To further establish whether genes differentially expressed upon Rsl24d1 knockdown
325 are direct targets of these PTFs and PRC factors, we next examined the promoter regions
326 of these 529 genes for enrichment in binding sites for these factors. ChIP-Seq assays
327 performed in murine ESCs, which are available in the ChIP-Atlas database for 9 factors
328 (52), were analyzed to identify binding sites in the vicinity of transcription start sites
329 (TSS ± 1 kb, referred to as promoter regions) for either up- or downregulated genes
330 upon RSL24D1 depletion (Fig. 4C, Table 5). Interestingly, promoters from
331 downregulated genes showed a significant 2-fold enrichment in POU5F1 and NANOG
332 binding sites compared to upregulated genes, therefore supporting the hypothesis that
333 genes downregulated upon RSL24D1 knockdown are enriched in POU5F1- and NANOG-
334 regulated genes. In addition, the promoter regions of upregulated genes were
335 significantly enriched in binding sites for PRC1 and PRC2 factors compared to
336 downregulated genes (Fig. 4C). Strikingly, about half of the promoter regions of
337 upregulated genes were bound by EZH2 (48,9%), SUZ12 (56,4%), EED (36%) or RNF2
338 (58,4%) in murine ESCs, respectively (Table 5). These results further confirmed that
339 genes down- or upregulated upon RSL24D1 depletion are enriched in targets of
340 POU5F1/NANOG or EZH2/SUZ12/EED/RNF2, respectively.
341 PRC2 complexes are key epigenetic repressors responsible for the genome-wide
342 deposition of H3K27me2 and H3K27me3 marks to control early embryonic gene
343 expression patterns in ESCs (1, 7-9). Since a large proportion of down- and upregulated
344 genes were associated with PRC2 binding sites, we next analyzed the H3K27
345 methylation status, established in mouse ESCs (9), of the promoter regions (+/- 1kb
346 near TSS) of the 529 genes differentially expressed upon Rsl24d1 depletion
347 (Supplemental Fig. S4B). While H3K27me2 marks were not preferentially enriched near
348 the TSSs of differentially expressed genes, we found that the promoter regions of genes
349 affected by RSL24D1 depletion were less associated with H3K27me1 modifications
350 marking active transcription and were rather significantly enriched in H3K27me3
351 repressive modifications. These results suggest that the levels of H3K27me3 might be
352 altered when RSL24D1 is depleted. Accordingly, si-Rsl24d1 treated CGR8 cells displayed
353 lower levels of nuclear H3K27me3 compared to si-CTL treated cells (Supplemental Fig.
354 S4C), suggesting that some of the alterations in gene expression detected by RNA-seq
355 upon RSL24D1 knockdown may directly result from this reduction in global H3K27me3.

bioRxiv preprint doi: https://doi.org/10.1101/2021.05.27.443845; this version posted May 29, 2021. The copyright holder for this preprint (which was not certified by peer review) is the author/funder. All rights reserved. No reuse allowed without permission.

356 Finally, we compared RNA-seq predictions from si-Rsl24d1 ESCs with gene expression
357 profiling from EED and EZH2 knockout mouse ESCs, respectively (7, 8). Interestingly,
358 genes displaying an altered expression upon RSL24D1 depletion were enriched in genes
359 that are mis-regulated in EED$^{-/-}$ or EZH2$^{-/-}$ ESCs (Supplemental Fig. 4E). Strikingly, genes
360 with an expression profile that was similarly impaired in PRC2 mutant cells and
361 RSL24D1-depleted cells were predominantly upregulated or derepressed genes (Fig.
362 4E). Altogether these results suggest that genes up- or downregulated upon RSL24D1
363 knockdown are likely controlled by distinct molecular mechanisms. On the one hand,
364 downregulated genes are enriched in key PTF target genes, suggesting that the
365 transcriptional regulatory activities of POU5F1 and NANOG are decreased in si-Rsl24d1
366 treated ESCs. On the other hand, the enrichment of H3K27me3 sites and binding sites
367 for PRC2 proteins in promoter regions of upregulated genes suggests that RSL24D1
368 depletion most likely hinders the repressive activity of PRC2. This results in lower
369 H3K27me3 deposition, therefore leading to the premature activation of developmental
370 genes normally silent in pluripotent ESCs.
371

372 *The translational regulation of key stemness factors is impaired upon RSL24D1 depletion*
373 *in mouse ESCs.*

374 In order to investigate how RSL24D1 depletion could affect the activity of PTFs and
375 PRC2 factors, we first measured whether the loss of RSL24D1 affected their
376 transcription. Interestingly, the expression of these PTFs and PRC factors was not
377 strongly impaired at the RNA level in si-Rsl24d1 ESCs, except for Nanog (Supplemental
378 Fig. S5A), suggesting that rather the production and/or the activity of the corresponding
379 proteins might be affected upon RSL24D1 depletion.
380 Since RSL24D1 depletion decreases global protein synthesis, we hypothesized that the
381 alteration of PRC2 activity could result from a perturbation of Eed, Ezh2 and Suz12
382 mRNA translation. To address this question, mRNAs associated with the different
383 ribosomal fractions, and in particular with actively translating ribosomes (i. e.
384 polysomes), were analyzed by RT-qPCR assays in CGR8 cells treated with either si-CTL
385 or si-Rsl24d1 (Supplemental Fig. S5B and S5C). As previously described, downregulating
386 RSL24D1 in ESCs impaired the accumulation of the cytoplasmic 40S, 60S and 80S
387 ribosome fractions (Supplemental Fig. S5B). As expected, the majority (>92%) of Eed,
388 Ezh2 and Suz12 mRNAs detected in this assay were associated with ribosome fractions

bioRxiv preprint doi: https://doi.org/10.1101/2021.05.27.443845; this version posted May 29, 2021. The copyright holder for this preprint (which was not certified by peer review) is the author/funder. All rights reserved. No reuse allowed without permission.

389 corresponding to polysomes suggesting that these mRNAs were actively translated in
390 self-renewing ESCs (Fig. 5A and Supplemental Fig. S5C, gray curves). However, in
391 RSL24D1-depleted cells, the association of Eed and Ezh2 mRNAs with polysomal
392 fractions was significantly reduced and correlated to an increased detection in fractions
393 corresponding to free mRNPs and monosomes (Fig. 5A and Supplemental Fig. S5C, black
394 bar graphs). In contrast, the polysome versus free mRNPs/monosome comparison was
395 not statistically significant for Suz12 mRNAs (Fig. 5A), in particular due to a biological
396 variability in the detection of these mRNAs throughout gradients. However, analyses of
397 the polysome fractions alone seemed to indicate that Suz12 mRNAs also tend to transit
398 from heavy to light polysomes upon RSL24D1 depletion (Supplemental Fig. S5C).
399 To further confirm that RSL24D1 downregulation impaired the translation of Suz12, Eed
400 and Ezh2 mRNAs, steady-state expression levels of the corresponding proteins were
401 assessed by semi-quantitative western blots from CGR8 total cell extracts. Interestingly,
402 RSL24D1 downregulation induced a significant reduction in the accumulation of EED
403 and SUZ12 proteins, albeit no significant decrease in expression was observed for EZH2
404 (Fig. 5B). Altogether, these observations suggest that the loss of PRC2 activity upon
405 RSL24D1 depletion, which may cause both a defect in H3K27me3 and an upregulation of
406 specific gene programs associated with development and differentiation, is likely caused
407 by a defect in the translation of Eed, Ezh2 and Suz12 mRNAs.
408 Similar to PRC2 factors, we hypothesized that a translational decrease of POU5F1 and
409 NANOG mRNAs may be responsible for the downregulation of specific genetic programs
410 enriched in POU5F1 and NANOG target genes. This hypothesis was indeed confirmed by
411 semi-quantitative western blots that demonstrated a significant reduction in the
412 detection of both POU5F1 and NANOG proteins in si-Rsl24d1 treated cells compared to
413 si-CTL cells (Fig. 5C). Immunostaining experiments confirmed a global and significant
414 loss of POU5F1 expression in si-Rsl24d1-treated ESCs suggesting that the POU5F1
415 downregulation previously observed by western blot in total cell extracts did not result
416 from the emergence of POU5F1 negative cells in ESC colonies but rather resulted from a
417 global decrease in POU5F1 expression (Supplemental Fig. S5D). Altogether, these results
418 confirm that RSL24D1 depletion directly impairs the translation and the accumulation of
419 both key PTFs and core PRC2 factors, which respectively play pivotal roles in controlling
420 gene expression programs and the chromatin landscape underlying cell fate decisions in
421 pluripotent ESCs.

bioRxiv preprint doi: https://doi.org/10.1101/2021.05.27.443845; this version posted May 29, 2021. The copyright holder for this preprint (which was not certified by peer review) is the author/funder. All rights reserved. No reuse allowed without permission.

422

423 *High RSL24D1 expression supports the maintenance of self-renewal capacities but is*
424 *dispensable for ESC differentiation.*
425 Since transient RSL24D1 depletion altered the expression of several PTF target genes
426 and promoted the activation of genes involved in developmental programs, we
427 examined the functions of RSL24D1 for ESC fundamental self-renewal and
428 differentiation capacities. First, stable RSL24D1 downregulation by constitutively
429 expressed shRNAs significantly impaired, in a dose-dependent manner, the proliferation
430 of CGR8 cells in both real-time assays (Fig. 6A) and long-term kinetics of proliferation
431 (Fig. 6B). Accordingly, expression of sh-Rsl24d1-2 demonstrating the most significant
432 loss of RSL24D1 (Supplemental Fig. S3B and S6A) also correlated with the strongest
433 proliferation impact on CGR8 cells (Fig. 6A and 6B). Considering that ESC self-renewal
434 capacities are tightly controlled at the molecular level by key transcriptional programs,
435 we next analyzed the expression of several major PTFs upon stable depletion of
436 RSL24D1 in CGR8 cells. In contrast to si-Rsl24d1 transient knockdowns, RT-qPCR assays
437 revealed a significant downregulation, at the mRNA level, of Nanog, Pou5f1 and Sox2 in
438 cells expressing the sh-Rsl24d1-2 sequence while Klf4 expression remained unaffected
439 (Supplemental Fig. S6A). The expression of the shRsl24d1-1 sequence induced a lower
440 depletion of RSL24D1 correlated to less pronounced alterations of these PTFs, with only
441 Sox2 being downregulated and Klf4 slightly upregulated (Supplemental Fig. S6A). Using
442 western blot assays, a significant downregulation of POU5F1 was also confirmed in sh-
443 Rsl24d1-2 expressing CGR8 cells (Supplemental Fig. S6B), suggesting that RSL24D1
444 stable depletion likely affected ESC self-renewal capacities. To determine whether this is
445 the case, CGR8 cells expressing non-targeting shRNAs (sh-Control), or shRNAs
446 specifically targeting Pou5f1 or Rsl24d1 mRNAs were seeded at clonal density to
447 recapitulate the formation of individual undifferentiated colonies displaying high levels
448 of alkaline phosphate (AP) activity (53). As expected from its key role in controlling ESC
449 self-renewal transcriptional programs, POU5F1 downregulation led to a drastic
450 reduction (>90 %) in the number of AP positive colonies compared to control shRNA
451 treated cells (Fig. 6C and Supplemental Fig. S6C). Similarly, RSL24D1 depletion caused a
452 dose-dependent and significant reduction (>50%) of AP-positive ESC colonies (Fig. 6C
453 and Supplemental Fig. S6C), suggesting that a high expression of RSL24D1 in mouse
454 ESCs is required to support both self-renewal and proliferation.

bioRxiv preprint doi: https://doi.org/10.1101/2021.05.27.443845; this version posted May 29, 2021. The copyright holder for this preprint (which was not certified by peer review) is the author/funder. All rights reserved. No reuse allowed without permission.

455 Finally, we compared the differentiation capacities of sh-Control, sh-Pou5f1 and sh-
456 Rsl24d1-1/2 expressing CGR8 cells by EB differentiation assays. As expected, POU5F1
457 knockdown strongly impaired the capacities of CGR8 cells to form viable 10 day-old EBs,
458 whereas RSL24D1 downregulation had no significant impact on EB formation compared
459 to sh-Control ESCs (Fig. 6D). We next assessed the functional differentiation of EB-
460 forming cells by counting the proportion of EBs displaying spontaneous beatings, which
461 characterize the presence of fully differentiated cardiomyocytes (54). This analysis
462 revealed that POU5F1 depletion almost completely abolished EB beating (Fig. 6E), likely
463 reflecting its role in early cell fate determination (55-57). Conversely, RSL24D1 stable
464 knockdowns only partially impaired the formation of functional cardiomyocytes after 10
465 days of differentiation (Fig. 6E). Thus, the depletion of RSL24D1 affects ESC self-renewal
466 and proliferation capacities but does not seem however to significantly interfere with
467 the processing of differentiation.
468

469 **Discussion**

470 Despite displaying reduced translation activity compared to differentiated progenies
471 (16, 17, 19), ESCs have also been previously shown to paradoxically express RBFs and
472 RPs at higher levels than differentiated cells (28, 30, 31, 58). These observations
473 therefore suggest that naive ESCs may need to accumulate, at a steady-state level, a pool
474 of ribosomes sufficient to sustain the rapid proteome changes and increased
475 translational activities required to achieve all possible programs of differentiation in
476 response to environmental signals. In order to better define the molecular mechanisms
477 and factors coordinating the highly regulated ribosome production in ESCs, we first
478 identified RBFs enriched in naive ESCs compared to differentiated cells. Our study
479 revealed that RSL24D1, a homolog of the yeast Rlp24 LSU ribosome biogenesis factor, is
480 consistently expressed at high levels in PSCs, including mouse ESCs and iPSCs, and is
481 rapidly downregulated after differentiation induction.

482 Since RSL24D1 function was not established in higher eukaryotes, we next
483 determined that RSL24D1 is predominantly localized in nucleoli, which are nuclear
484 domains playing a central role in the transcription and maturation of pre-rRNAs (59).
485 Considering the strong conservation of RSL24D1 structure and functions relative to its
486 yeast homolog Rlp24, it is also likely that RSL24D1 shuttles between the nucleus and the
487 cytoplasm (42). Accordingly, immunostaining assays revealed that, while the majority of

bioRxiv preprint doi: https://doi.org/10.1101/2021.05.27.443845; this version posted May 29, 2021. The copyright holder for this preprint (which was not certified by peer review) is the author/funder. All rights reserved. No reuse allowed without permission.

488 endogenous RSL24D1 is detected in the nucleoli of mouse ESCs (Fig. 2B), RSL24D1
489 signals are also detected in the cytoplasm, in contrast with FBL signals strictly detected
490 in the nucleoli. Conversely, RPL24 is almost exclusively present in the cytoplasm as
491 described in yeast (42). In yeast, Rlp24 is assembled at the initial steps of pre-60S
492 maturation corresponding to the state B (60), together with Tif6, Nog1 and Mak11 (23,
493 61), and then allows the recruitment of the hexameric Drg1 AAA-ATPase (42, 62). As the
494 particles exit the nucleus, Drg1 gets activated by nucleoporins and releases Rlp24 from
495 the pre-60S by mechanical force (42, 62-64), therefore allowing its substitution by the
496 canonical ribosomal protein Rpl24. Although the loss of Rlp24 in yeast induced
497 moderate alterations of the 35S and 27SB rRNA intermediates, we did not observe any
498 significant modifications of the rRNA processing in mouse ESCs treated with siRNAs
499 targeting Rsl24d1 mRNAs (data not shown). Even though this observation may reflect a
500 difference in the efficacy of RSL24D1/Rlp24 depletions in each model, both the
501 conditional Rlp24 mutant in yeast (42) and the depletion of RSL24D1 in human cells
502 (65) did not strongly impact the accumulation of maturation intermediates or mature
503 LSU rRNAs. These observations indeed suggest that RSL24D1 rather guides the
504 association of other proteins to early states of pre-60S, in particular Tif6, the yeast
505 homolog of EIF6, rather than regulating early exonucleolytic and endonucleolytic rRNA
506 processing (42, 60, 66). Consistently, the depletion of RSL24D1 in mouse ESCs is
507 correlated to a loss of EIF6 association to nuclear pre-ribosomes (Fig. 3D). Interestingly,
508 RSL24D1 and EIF6 show different dynamics of disassembly from cytoplasmic
509 ribosomes, consistent with their dynamics of assembly/release in yeast (Fig. 2C). EIF6
510 dissociation seems to occur belatedly as it is more stably associated with cytoplasmic
511 ribosomal particles. These observations are therefore consistent with the yeast model
512 describing Tif6 removal as the latest maturation step of 60S particles (23, 67).
513 Furthermore, yeast Rlp24 has a key protein-protein mimicry role during pre-60S
514 maturation until it is replaced, after nuclear export of pre-LSU particles, by the canonical
515 Rpl24, which is strictly localized to the cytoplasm (42). Our data strongly support a
516 conserved mimicry function for RSL24D1 in mouse ESCs as its depletion impairs the
517 association of RPL24 with cytoplasmic ribosomes (Fig. 3D).
518 Moreover, consistent with a conserved role in the LSU biogenesis, RSL24D1 depletion in
519 mouse ESCs caused a loss of 60S and 80S subunits relative to 40S particles. A similar
520 imbalance of the accumulation of 60S and 80S over 40S subunits was previously

bioRxiv preprint doi: https://doi.org/10.1101/2021.05.27.443845; this version posted May 29, 2021. The copyright holder for this preprint (which was not certified by peer review) is the author/funder. All rights reserved. No reuse allowed without permission.

521 observed in yeast upon Rlp24 depletion (42) or 60S biogenesis repression (33, 68). In
522 addition, we detected the presence of half-mers for di- and tri-ribosomes in si-Rsl24d1
523 treated cells (Figure 3B), which were previously observed upon LSU biogenesis
524 alterations in yeast (69, 70). Finally, RSL24D1 has also been detected in nuclear pre-60S
525 cryo-structures while it is absent from cytoplasmic pre-LSU in human cells and we
526 demonstrated that RSL24D1 expression profile is also conserved in human ESCs, further
527 supporting a conserved molecular function in ribosome biogenesis and stem cells
528 throughout evolution.

529 We then established that RSL24D1 depletion, in addition to impairing the
530 accumulation of 60S subunits in the cytoplasm, also strongly alters global translation in
531 naive CGR8 cells. This result agrees with previous observations that the loss of
532 expression of either HTATSF1, which controls rRNA processing, or SSU biogenesis
533 factors also impair translation in mouse ESCs (21, 31). In addition to a global
534 translational impact, we provided evidence that RSL24D1 depletion is correlated to a
535 reduced expression of specific instable proteins including POU5F1 and NANOG. It is
536 worth noting that the decrease in NANOG expression may result from a combination of
537 both transcriptional and translation defects while POU5F1 downregulation was not
538 detected at the transcriptional level in the same conditions (Fig. 5C and Supplemental
539 Fig. 5A). A highlight of this study is that the steady-state level of several PRC2 factors,
540 including EZH2, EED and SUZ12 is tightly controlled by the level of ribosome biogenesis
541 in ESCs. Although these factors play a key role in organizing the landscape of active and
542 transcriptionally silent chromatin, and are essential to repress developmental genes by
543 maintaining H3K27me3 modifications on promoter regions, their activity rather seems
544 rate-limiting as slight changes in expression have a massive impact on global gene
545 regulation in ESCs. Indeed, the downregulation of RSL24D1 in mouse ESCs induced a
546 reduction in Eed, Suz12 and Ezh2 mRNAs association to polysomes, which is predicted
547 to have a direct impact on corresponding neosynthesized proteins. Accordingly, despite
548 RSL24D1 depletion causing a reduction ranging from 7% to 35% in corresponding EED,
549 SUZ12 and EZH2 protein levels, we observed a correlated and significant increased
550 expression, at the transcriptional levels, of hundreds of PRC2 target genes normally
551 associated to repressive H3K27me3 marks. Many of these PRC2 target genes correspond
552 to developmental genes, including members of the HOX (HOXB1, 2, 3, 9 and C13) and
553 WNT families (WNT2B, 3, 10A and 10B), transcription factors such as NKX1-2, NKX2-9,

bioRxiv preprint doi: https://doi.org/10.1101/2021.05.27.443845; this version posted May 29, 2021. The copyright holder for this preprint (which was not certified by peer review) is the author/funder. All rights reserved. No reuse allowed without permission.

554 POU4F3, SALL3 and NEUROD1. Altogether, this therefore suggests that the versatile
555 status of ESCs, which must rapidly switch from a transcriptionally active self-renewal
556 program to the activation of poised developmental or differentiation programs, requires
557 a finely tuned translation of PRC2 factors that is coordinated with ribosome biogenesis
558 in ESCs.

559 At the physiological level, we showed that RSL24D1 depletion caused a
560 significant loss of proliferation and self-renewal capacity while having a moderate
561 impact on ESC differentiation *in vitro*. This is in agreement with RSL24D1 expression
562 profile, which is high in ground state and naive pluripotent ESCs but low in
563 differentiating progenies, therefore supporting the hypothesis that RSL24D1 expression
564 is required for ESC maintenance. Surprisingly, attempts to overexpress an exogenous
565 FLAG-RSL24D1 protein at near ESC endogenous levels, induced a rapid and stable
566 downregulation of the endogenous RSL24D1 in ESCs (data not shown). This therefore
567 suggests that PSCs finely tune the steady-state level of RSL24D1, most likely to avoid
568 aberrant RSL24D1 levels that could be detrimental for ribosome biogenesis and stem
569 cell homeostasis.

570 Altogether, we propose a model where RSL24D1 actively contributes to the
571 biogenesis of pre-60S ribosomal particles and to the accumulation of mature
572 monosomes and polysomes in the cytoplasm of naive mouse ESCs (Fig. 7). We suggest
573 that RSL24D1 shuttles back and forth between the nucleoli and the cytoplasm to support
574 an elevated rate of 60S biogenesis in ESCs while its activity is less required in
575 differentiating ESC progenies. Here, we demonstrated for the first time that the
576 expression of a RBF of the LSU is regulated as ESCs transition from naive to
577 differentiated states, and is required to maintain ESC self-renewal and proliferation.
578 Interestingly, RSL24D1-mediated ribosome biogenesis therefore appears to have a dual
579 role in controlling ESC self-renewal. On the one hand, RSL24D1 maintains a balanced
580 expression of key PTFs, including POU5F1 and NANOG, to control pluripotency
581 transcriptional programs. Furthermore, RSL24D1 expression profile is correlated to
582 POU5F1 expression during CGR8 differentiation (Supplemental Fig. 1C), and RSL24D1 is
583 a predicted target gene of POU5F1 (Table S4 and ChIP-Atlas database) and NANOG
584 (ChIP-Atlas database). The stable depletion of POU5F1 by shRNAs is correlated to a
585 significant reduction (>60%, data not shown) in RSL24D1 expression at the mRNA and
586 protein levels in CGR8, suggesting that RSL24D1 expression could be directly controlled

bioRxiv preprint doi: https://doi.org/10.1101/2021.05.27.443845; this version posted May 29, 2021. The copyright holder for this preprint (which was not certified by peer review) is the author/funder. All rights reserved. No reuse allowed without permission.

587 by POU5F1 or NANOG in mouse ESCs. On the other hand, RSL24D1 sustains steady-state
588 translation of PRC2 factors and therefore maintains repressive H3K27me3 chromatin
589 marks to prevent the premature activation of developmental genes in naive ESCs (Fig.
590 7). Intriguingly, EZH2 was recently shown to have a PRC2-independent function by
591 promoting the interaction between NOP56 and FBL in human cancer cells and mouse
592 extraembryonic endoderm stem cells, and enhancing 2'-O-methylation of rRNAs (71).
593 This observation raises the question of whether RSL24D1 might influence rRNA 2'-O-
594 methylation by differentially modulating EZH2 expression in naive and differentiated
595 ESCs. Altogether, these results therefore further support that RSL24D1 may be at the
596 core of a regulatory loop that engages the regulation of ribosome biogenesis and
597 translation with chromatin epigenetic and transcription regulations in order to precisely
598 control ESC self-renewal and pluripotency properties.

599 Finally, modulating the production of ribosomes might not only impact global
600 translation but could also be a mechanism to control the translation of specific subsets
601 of mRNAs that regulate ESC fate. Indeed, it is puzzling that despite an active ribosome
602 biogenesis, ESCs display a globally reduced translational activity, which is correlated to
603 a relatively small cytoplasm compared to differentiated cells. A first hypothesis could be
604 that mouse ESCs have a short cell cycle and therefore an elevated cell division rate that
605 could stimulate ribosome biogenesis. However, whether all the ribosomes present in
606 PSCs are actively engaged in translation still remains to be established. Another
607 seducing hypothesis to explain this discrepancy may be that the ribosome concentration
608 may regulate substrate selectivity and that maintaining a high ribosome biogenesis, and
609 therefore concentration allows the translation of specific programs. This "Ribosome
610 Concentration" model has been previously discussed (72) and may explain why the
611 translation of ESC-relevant mRNAs requires such an elevated amount of ribosomes. One
612 could therefore speculate that fluctuations of ribosome biogenesis, i.e. upon RSL24D1
613 expression decrease, could affect specific translation programs. Consistently, several
614 observations indicate that upstream open reading frames (uORFs) are commonly used
615 in naive ESCs compared to differentiated cells (73), and that the mRNAs coding for key
616 PTFs, including Nanog, possess multiple uORFs which specifically enhance their
617 translation in ESCs (74). Hence, uORF-carrying mRNAs may require a certain amount of
618 ribosomes to be correctly translated in the context of ESCs while other non-uORF mRNA
619 may be repressed in this context. Transposed to the ESC model which naturally

bioRxiv preprint doi: https://doi.org/10.1101/2021.05.27.443845; this version posted May 29, 2021. The copyright holder for this preprint (which was not certified by peer review) is the author/funder. All rights reserved. No reuse allowed without permission.

620 modulates the production of ribosomes depending on their cellular fate, one could
621 propose that naive and differentiating ESCs differentially modulate the translation of
622 specific populations of mRNAs in addition to the global regulation of translation, as a
623 mean to control specific gene programs, such as Nanog-dependent pluripotency or
624 PRC2-dependent differentiation programs. Along these lines, the direct impact of
625 ribosomes on gene-specific regulations has been highlighted in the context of congenital
626 diseases, the ribosomopathies, which are caused by mutations in RBFs or RPs, and
627 characterized by quite heterogeneous phenotypes ranging from specific developmental
628 alterations to increased risks of cancer (72). Therefore, better defining the molecular
629 feedbacks between ribosome biogenesis, translation and additional key steps of gene
630 expression, including chromatin modifications and transcription, could not only benefit
631 to a developmental research but also to open novel avenues to consider disease
632 treatments.
633
634
635 **Materials and methods**
636
637 **RNA-seq datasets**
638 RNA-seq data for mouse pluripotent cells, differentiated cells and tissues were obtained
639 from a previously published dataset (GSE45505) (36).
640
641 **Cell culture**
642 CGR8 mouse embryonic stem cells (ECACC General Collection, 07032901) were cultured
643 on 0.2% gelatin-coated plates either in ESC^{FBS} conditions using GMEM BHK-21 (Gibco)
644 supplemented with 10% ESC-grade heat-inactivated Fetal Bovine Serum (FBS), 1x non-
645 essential amino acid (Gibco), 2 mM Sodium Pyruvate (Gibco), 100µM β-mercaptoethanol
646 (BME, Sigma-Aldrich), 10^3U/ml Leukemia Inhibitory Factor (LIF, StemCells
647 Technologies) or in ESC^{2i} conditions using 45% DMEM/F12 (Gibco), 45% Neurobasal
648 medium (Gibco), 100µM BME, 1.65% Bovine Serum Albumin Fraction V (Gibco), 1X
649 penicillin-streptomycin (Gibco), 1% N2 supplement (Gibco), 2% B27 supplement
650 (Gibco), 1X ESGRO 2i supplement (MEK1/2, GSK3β inhibitors, Millipore) and 10^3U/ml
651 Leukemia Inhibitory Factor (Millipore).

bioRxiv preprint doi: https://doi.org/10.1101/2021.05.27.443845; this version posted May 29, 2021. The copyright holder for this preprint (which was not certified by peer review) is the author/funder. All rights reserved. No reuse allowed without permission.

652 The mouse ESC lines R1 (ATCC-SCRC-1011) and G4 (RRID:CVCL_E222) were cultured on
653 irradiated mouse embryonic fibroblasts, in High Glucose DMEM (Gibco), 10% ESC-grade
654 heat-inactivated FBS, 1X non-essential amino acid, 1mM Sodium Pyruvate, 100µM BME
655 and 10^3U/ml LIF.
656 H9 and OSCAR human embryonic stem cells were cultured as previously described (41)
657 and were provided by the Savatier laboratory from the Stem cell and Brain Research
658 Institute (Inserm U1028), 69500 Bron, France.
659 HEK-293T cells were cultured in DMEM (Invitrogen) supplemented with 10% heat
660 inactivated FBS (Sigma-Aldrich), 1X non-essential amino acid, 2mM Sodium Pyruvate
661 and 1X penicillin-streptomycin.
662 All cell lines used in the study were confirmed mycoplasma-free (Lonza, MycoAlert kit).
663

664 **MEF reprogramming into iPSCs**

665 MEFs were isolated from R26^{rtTA};Col1a1^{4F2A} E13.5 embryos after removal of the head
666 and internal organs (75). The remaining tissues were physically dissociated and
667 incubated in trypsin 10 minutes at 37°C. Dissociated cells were resuspended in MEF
668 medium (DMEM supplemented with 10% fetal bovine serum, 100 U/mL penicillin /
669 streptomycin, 1mM sodium pyruvate, 2mM L-glutamine, 0.1mM Non Essential Amino
670 Acids and 0.1mM β-mercaptoethanol).
671 To induce the reprogramming process, MEFs were plated in six-well plates at 80,000-
672 100,000 cells per well in MEF medium (75). The following day the medium was replaced
673 by fresh MEF medium containing 2µg/mL doxycyclin. MEFs were reseeded after 72h on
674 0.1% gelatin-coated plates in iPSC medium (DMEM containing 15% KnockOut Serum
675 Replacement, 1,000 U/mL leukemia inhibitory factor, 100 U/mL penicillin /
676 streptomycin, 1mM sodium pyruvate, 2mM L-glutamine, 0.1mM Non Essential Amino
677 Acids and 0.1mM β-mercaptoethanol). Every day, medium was either replaced by or
678 supplemented with doxycyclin-containing fresh medium.
679 After 14 days of reprogramming, iPS colonies are picked individually, amplified and
680 maintained for several passages.
681

682 **Differentiation assays**

683 Embryoid body (EB) formation assays were performed by the hanging drop method (76,
684 77). Briefly 400 cells were cultured in 20 µL hanging drops for 2 days in GMEM BHK-21

bioRxiv preprint doi: https://doi.org/10.1101/2021.05.27.443845; this version posted May 29, 2021. The copyright holder for this preprint (which was not certified by peer review) is the author/funder. All rights reserved. No reuse allowed without permission.

685 supplemented with 20% heat-inactivated FBS, 1x non-essential amino acid, 2mM
686 Sodium Pyruvate, 100μM BME. EBs were then collected in non-adherent culture dishes
687 and cultured for 3 additional days. At Day 5, cell aggregates were cultured on 0.2%
688 gelatin-coated dishes in the presence of 10nM retinoic acid (Sigma-Aldrich) and the
689 media was changed every 2 days.
690
691 **Plasmids**
692 pLKO.1-puro plasmids (Addgene #8453) were cloned as previously described (78).
693 Briefly, the pLKO.1 plasmid was digested with EcoRI and AgeI restriction enzymes.
694 Linear plasmids were ligated with annealed oligomers containing the shRNA sequence
695 flanked by EcoRI and AgeI restriction sites, respectively. All clones were sequenced to
696 confirm the insertion of each shRNA sequence in the pLKO.1 backbone prior to lentiviral
697 production.
698
699 **Lentiviral production and infection:**
700 The production of lentiviral particles for shRNA expression was performed as previously
701 described (79, 80). Briefly, HEK-293T cells were co-transfected with corresponding
702 pLKO.1 plamids and 3rd generation packaging lentiviral plasmids (pLP1, pLP2, pLP-
703 VSVG) using FuGENE HD (Promega), according to the manufacturer's recommendations.
704 Cell media containing lentiviral particles were concentrated using centricon column
705 (Vivaspin 20, Sartorius). Each viral production was titrated beforehand to establish a
706 multiplicity of infection (MOI) sufficient to provide a complete resistance to 1.5 μg/mL
707 of puromycin (Sigma-Aldrich).
708 ESCs were infected with an MOI=1 for 16 hours in ESC^{FBS} conditions supplemented with
709 polybrene at 8 μg/mL (Sigma-Aldrich). 24h after infection, cells were selected with 1.5
710 μg/mL of puromycin for at least 48 hours. shRNA sequences used in this study are
711 reported in Table S6A.
712
713 **siRNA Transfection**
714 ESCs were transfected with 20nM siRNAs using DharmaFECT 1 transfection reagent
715 (Horizon Discovery) according to the manufacturer's protocol, for the indicated times in
716 ESC^{FBS} conditions. Negative control pool (D-001810-10-20, ON-TARGETplus, Horizon
717 Discovery) was used as a negative control for siRNA transfection while RSL24D1

bioRxiv preprint doi: https://doi.org/10.1101/2021.05.27.443845; this version posted May 29, 2021. The copyright holder for this preprint (which was not certified by peer review) is the author/funder. All rights reserved. No reuse allowed without permission.

718 knockdowns were achieved using ON-TARGETplus RSL24D1 SMARTpool (L-054445-01-
719 0010, Horizon Discovery).
720

721 **Colony-formation assay**

722 ESCs were plated at clonal density (60 to 100 cells per cm2) on gelatin-coated plates in
723 ESC^{FBS} conditions. The medium was changed every two days for seven days before
724 detection of alkaline phosphatase-positive colonies (Alkaline Phosphatase detection kit,
725 Merck-Millipore). Alkaline phosphatase-positive colonies were analyzed and quantified
726 using ImageJ analysis software (81).
727

728 **Proliferation assays**

729 The proliferation was first assessed using the x-CELLigence Real-Time Cell Analysis
730 (RTCA) system (ACEA Biosciences, San Diego, CA, USA). 5000 cells were seeded in a 96
731 E-plates (Roche) and the electrical impedance was acquired every 15 minutes for seven
732 days to establish a cell index value extracted from the linear regression of the
733 proliferation curve. The data were analyzed by RTCA software.
734 In addition, the proliferation was also monitored using the high-definition automated
735 imaging system IncuCyte (Essen BioScience), according to the manufacturer's
736 instructions. 750 infected and selected cells were seeded in a 24-well plate, with 2-hour
737 interval snapshots. Proliferation rates were estimated according to the manufacturer's
738 insctructions.
739

740 **Western Blots**

741 Cells were lysed in 1x Laemli buffer (50mM Tris-HCl pH 6.8, 2% SDS, 5% BME, 10%
742 glycerol and 0.05% bromophenol blue) and analyzed by SDS-polyacrylamide gel
743 electrophoresis and western blotting using antibodies indicated in Table S7B.
744 For total protein quantification, 0.5% trichloroethanol (Sigma-Aldrich) was included in
745 the SDS-polyacrylamide gel prior to electrophoresis and activated post-electrophoresis
746 with UV light for 45s. Chemiluminescent and fluorescent signals were acquired on
747 ChemiTouch MP imaging system (Bio-rad) and quantified using ImageLab software
748 (Bio-rad) by normalizing signals of interest to housekeeping protein (β-actin, GAPDH) or
749 total protein signals. Serial sample dilutions were systematically loaded onto gels and
750 analyzed to verify the linearity of quantified signals.

bioRxiv preprint doi: https://doi.org/10.1101/2021.05.27.443845; this version posted May 29, 2021. The copyright holder for this preprint (which was not certified by peer review) is the author/funder. All rights reserved. No reuse allowed without permission.

751

752 **Immunofluorescence assays and High-Content analysis System (HCS)**

753 ESCs were cultured in ESC^{FBS} conditions either on 0.2% gelatin-coated coverslip (SPL) or
754 gelatin-coated 96-well plates. 48 after siRNA transfections, ESCs were fixed for 10 min in
755 4% formaldehyde and permeabilized for 10 min in 0.1% Triton X-100. Cells were then
756 incubated 1 hour in blocking solution (1X PBS, 0.1% tween 20, 5% BSA) and then
757 incubated with primary and secondary antibodies indicated in Table 6B. Images were
758 acquired using a Zeiss Axio Imager M2 microscope coupled with the Zen 2 Pro software
759 (Zeiss) and processed with ImageJ.
760 For deeper statistical results, cells were plated on a 96 well carrier plate (Perkin Elmer)
761 optimized for sensitive and resolved fluorescence microscopy. At least 90% of the well
762 surface is acquired in one non-confocal plane with Harmony software on an Operetta
763 CLS Flex High-content-Screening system (Perkin Elmer) equipped with 20x/NA1.0
764 water objective. The set-up was optimized to reach at least a difference of 10000
765 fluorescence levels between the noise and the signal of interest to allow a robust images
766 analysis and quantification. Data were analyzed with Columbus software (Perkin Elmer).
767 Briefly, on the image of full wells, colonies were located on the nuclei labeling with the
768 appropriate tuned find image region algorithm. To discard small and large colonies,
769 areas in the range of 500 to 40 000 μm^2 of cells were selected. Then cells in each colony
770 were found with the appropriate tuned find nuclei algorithm. Cell debris and objects
771 with more than one nucleus were excluded by filtering the nuclei according to
772 roundness and surface. Fluorescence intensities are calculated for each selected cellular
773 region for all wells.

774

775 **Cell fractionation**

776 ESCs were collected by trypsinisation and gently lysed for 10 min on ice in hypotonic
777 buffer (HB) containing 10 mM KCl, 0.5 mM $MgCl_2$, 10 mM Tris-HCL pH 7.4, 1X cOmplete
778 EDTA-free protease inhibitors™ (Roche) and 1U/µL RNAseOUT (Invitrogen). 0.02% NP-
779 40 was subsequently added for 5 more minutes and nuclei and cytoplasm were then
780 separated through sequential centrifugations. Nuclei were washed with HB
781 supplemented with 0.01% NP-40 and resuspended in Buffer A (250 mM Saccharose, 250
782 mM KCl, 5mM $MgCl_2$ and 50mM Tris-HCl pH7.4) with DNAse I (2000U/mL). Cytoplasmic
783 fractions in HB were adjusted to 250 mM KCL.

bioRxiv preprint doi: https://doi.org/10.1101/2021.05.27.443845; this version posted May 29, 2021. The copyright holder for this preprint (which was not certified by peer review) is the author/funder. All rights reserved. No reuse allowed without permission.

784

785 **Ribosome purification on sucrose cushion**

786 Cytoplasmic and nuclear fractions were loaded on 1 mL sucrose cushion (1M
787 saccharose, 250mM KCl, 5mM $MgCl_2$ and 50mM Tris HCl pH7.4) and centrifugated at
788 250.000 g for 2 hours at 4°C. Pellets were washed twice with cold water and
789 resuspended in Buffer C (25mM KCl, 5mM $MgCl_2$ and 50 mM Tris-HCl pH 7.4).

790

791 **Polysome profiling**

792 ESCs were treated with 25 µg/mL of emetine (Sigma-Aldrich) for 15 min and lysed in 10
793 mM Tris-HCL pH7.5, 5 mM $MgCl_2$, 100 mM KCl, 1% Triton X-100, 2 mM DTT, 1U/µL
794 RNAseOUT and 2X cOmplete EDTA-Free protease inhibitors. Lysates were centrifugated
795 at 1300 g for 10 min to pellet nuclei. Supernatants corresponding to cytoplasmic
796 fractions were then loaded on 10%-50% sucrose gradients poured using the Gradient
797 Master (Serlabo Technologies) and centrifugated at 210.000 g for 2h35 at 4°C. 700 µl
798 fractions were collected using the TELEDYNE ISCO collector while concomitantly
799 acquiring corresponding 254nm absorbance.

800

801 **RNA extraction**

802 *RNA extraction from cells* - Cells were harvested in 1ml of TRIzol reagent (Invitrogen)
803 and total RNA was extracted according to manufacturer's instructions. RNA
804 concentration was assessed with a Nanodrop 2000/2000c spectrophotometer
805 (ThermoScientific). 1 µg of RNA were used for reverse transcription assays using
806 SuperScript II reverse Transcriptase Mix (Invitrogen) according to manufacturer's
807 instructions.

808 *RNA extraction from sucrose gradients* - 50 pg of LUCIFERASE RNA (Promega) was added
809 to 250 µl of fractions collected from sucrose gradients. 750 µl of TRIzol LS (Invitrogen)
810 was then added and RNA was extracted according to the manufacturer's instructions.
811 The cDNAs were synthetized using SuperScript™ II Reverse Transcriptase (Invitrogen).

812

813 **Real Time qPCR assays**

814 Quantitative PCR experiments were performed using SYBR Green Technology (Roche,
815 Applied Biosystem) following the manufacturer's instructions. Relative cDNA expression
816 was normalized either by using mouse housekeeping gene encoding mRNAs β-Actin,

bioRxiv preprint doi: https://doi.org/10.1101/2021.05.27.443845; this version posted May 29, 2021. The copyright holder for this preprint (which was not certified by peer review) is the author/funder. All rights reserved. No reuse allowed without permission.

817 Psmd9, Tbp and 603B20Rik (total cell RNA) or by using Luciferase mRNAs (sucrose
818 gradient RNA). Serial dilutions were systematically performed to calculate qPCR
819 efficiency, verify the qPCR linearity and determine normalized relative cDNA
820 concentrations. Primers used in this study are listed in Table 6C.
821
822 **Metabolic labeling of protein synthesis.**
823 Cells were transfected with siRNAs in 6-well plates 48h before metabolic labelling. For
824 labelling, the cells were incubated for 5 minutes at 37°C with 55µCi/well of 35S-L-
825 methionine and ^{35}S-L-cysteine Promix (Perkin Elmer) in a minimal volume of culture
826 medium. To validate the labelling efficiency, a control was performed by incubating the
827 cells with cycloheximide (100mg/mL final) for 10 min prior to labelling. After
828 incubation, the cells were washed with 1 ml of ice-cold PBS and lysed in 500µL of RIPA
829 buffer mixed with 2X final LDS Novex™ 4X Bolt™ loading buffer (ThermoFisher) for
830 protein gel electrophoresis. Before loading onto precast Bis-Tris Bolt™ 4 to 12%
831 acrylamide gels (ThermoFisher), the samples were sonicated for 5 min and denatured at
832 70°C for 10 min. The Simply Blue Safestain (Thermo) kit was used to check if protein
833 loading was similar across lanes (accordingly to manufacturer's guidelines). After
834 coomassie staining, the gel was incubated in 30% ethanol, 10% acetic acid and 5%
835 glycerol for 1h. The gel was dried at 75°C for 1h30 and autoradioactivity levels were
836 then measured using the Typhoon Phosphor imager.
837
838 **Histone Immuno-histochemistry assays**
839 Cells were centrifugated during 10 min at 377g and fixed in an alcohol based fixative
840 solution Thinprep® (Hologic) during 15 min. After centrifugated during 5 min at 377g,
841 the cells were resuspended in 10ml of Epredia™ Gel (Richard-Allan Scientific™
842 HistoGel™). The gel was hardened during 15 min at 4°C and the corresponding blocks
843 were dehydrated and embedded in paraffin. 3µm-sections were immunostained using
844 an antibody anti-histone H3 containing the trimethylated lysine 27 (H3K27me3)
845 (Diagenode). Heat induced antigen retrieval was done using CC1 basic buffer (Ventana).
846 Staining was performed using DAB Ultraview dection system (Ventana).
847
848
849

bioRxiv preprint doi: https://doi.org/10.1101/2021.05.27.443845; this version posted May 29, 2021. The copyright holder for this preprint (which was not certified by peer review) is the author/funder. All rights reserved. No reuse allowed without permission.

850 **RPL24 and RLP24 homologs protein alignments.**

851 The following protein sequences were considered for protein alignments. For RLP24
852 homologs: *S. cerevisiae* (Q07915), *C. elegans* RLP24 (Q17606), *D. rerio* RLP24 (Q7ZTZ2),
853 *M. musculus* RSL24D1 (Q99L28), R. *norvegicus* RSL24D1 (Q6P6G7), *B. Taurus* RSL24D1
854 (Q3SZ12), *H. sapiens* RSL24D1 (Q9UHA3). For RL24 homologs: *S. cerevisiae* RL24A
855 (P04449), *S. cerevisae* RL24B (P24000), *M. musculus* RL24 (Q8BP67). Multiple protein
856 alignments were performed with the Clustal Omega software
857 (https://www.ebi.ac.uk/Tools/msa/clustalo/) (82) and visualized with the Jalview
858 software (http://www.jalview.org/) (83).

859

860 **RSL24D1 protein ternary structure predictions.**

861 The yeast RLP24 structures have been obtained from three yeast cryo-EM pre-60S
862 structures available in the Protein Data Bank (https://www.rcsb.org): PDB-6N8J
863 (residues 1-149, 2019, 3,50Å resolution) (45), PDB-6C0F (residues 2-130, 2018, 3,70Å
864 resolution) (43) and PDB-3JCT (residues 1-150, 2016, 3,08Å resolution) (44). The
865 mouse RSL24D1 protein structures have been modeled based on these 3 RLP24 cryo-EM
866 protein structures using the SWISS-MODEL structures assessment tool
867 (https://swissmodel.expasy.org/assess) (84-87) and respectively shared 61,48%
868 (amino acids 1-135), 55,63% (amino acids 2-130) and 61,48% (amino acids 1-135) of
869 homology with the yeast RLP24 protein sequence. The predicted mouse structures were
870 compared with structural models of human RSL24D1 proteins derived from the PDB-
871 6LSS and PDB-6LU8 pre-60S particle structures using the Pymol software.

872

873 **RNA-Seq sequencing and analysis.**

874 RNA libraries were prepared with the TruSeq Stranded Total-RNA kit and sequenced
875 using an Illumina NovaSeq 6000 sequencing machine. Raw sequencing data quality
876 controls were performed with FastQC (v 0.11.5). These data were aligned on the mouse
877 genome (GRCm38) with STAR (v2.7.0f), with the annotation of known genes from
878 gencode vM20, for careful quality control. RNA quality control metrics (library content,
879 GC content) were computed using RSeQC (v 3.0.0) (88).
880 Gene expression was quantified using Salmon (0.14.1) on the raw sequencing reads,
881 using the annotation of protein coding genes from gencode vM20 as index. Unless
882 otherwise specified, the analyses were performed using R (v3.6.1). Starting from salmon

bioRxiv preprint doi: https://doi.org/10.1101/2021.05.27.443845; this version posted May 29, 2021. The copyright holder for this preprint (which was not certified by peer review) is the author/funder. All rights reserved. No reuse allowed without permission.

883 transcript quantification, we used the R packages Tximport (v1.12.3) (89) DESeq2
884 (v1.24) (90) to perform the differential expression analyses (Wald test, and p-values
885 correction with the Benjamini-Hochberg method).
886

887 **GO enrichment analysis**

888 The analyses of overrepresented gene ontology categories were conducted using a
889 reference set of 15093 genes expressed in CGR8 cells and using BiNGO (v3.0.3) (91) as
890 well as the open source bioinformatics software platform Cytoscape (v3.7.2) (92) for
891 visualization of the results. Only annotations with a corrected p-value < 0.01 were
892 considered for further analysis (p-values corrections with the Benjamini-Hochberg
893 method).
894

895 **Target genes analysis with StemChecker**

896 Differentially expressed genes in Rsl24d1-depleted cells were analysed using the web-
897 server StemChecker (http://stemchecker.sysbiolab.eu/) (51), without masking the cell
898 proliferation and cell cycle genes.
899

900 **Analysis of binding sites defined by ChIP-seq**

901 To identify binding sites for TFs and chromatin-associated factors in the ±1 kb region of
902 TSSs, we combined all datasets available in the ChIP-Atlas database (52) corresponding
903 to mouse wild type ESCs and mouse differentiated cell types for each factor. To select
904 binding sites preferentially bound by the selected factors in ESCs, we selected all sites
905 with a ratio of ESC average score / Differentiated averaged score >2.
906

907 **Competing Interest Statement**

908 The authors declare no competing interests.
909

910 **Acknowledgments**

911 We thank Drs. P. Savatier and P.Y. Bourrillot (Stem cell and Brain Research Institute,
912 Lyon, France) for providing protein extracts of human ESCs, and Pr. A. Nagy (University
913 of Toronto, Canada) for providing the R1 and G4 cell lines. We thank R. Pommier and A.
914 Viari from the Gilles Thomas Bioinformatics Platform (CRCL, Lyon, France) for the
915 analysis of RNAseq data. This study was supported in part by a Marie Curie Career

bioRxiv preprint doi: https://doi.org/10.1101/2021.05.27.443845; this version posted May 29, 2021. The copyright holder for this preprint (which was not certified by peer review) is the author/funder. All rights reserved. No reuse allowed without permission.

916 Integration Grant 631794 from the European Union and by a national ATIP/AVENIR
917 grant from the Institut National de la Santé et de la Recherche Médicale (INSERM) to
918 M.G., and by a Ph.D. fellowship by La Ligue Nationale Contre le Cancer (M.B.), by grants
919 from Labellisation de la ligue contre le cancer, Agence Nationale pour la Recherche
920 (ANR) and Institut National du Cancer (INCa) (A.H. and F.L.).
921
922
923 **Author contributions:** S.D., M.B. and M.G. designed the research. S.D., M.B., F.B., B.B.,
924 J.B., C.I., A.H., D.M. performed the research. S.D., M.B., C.V., F.C., J.J.D., F.L, E.R., F.D. and
925 M.G. analyzed the data. S.D., M.B., F.B. and M.G. wrote the manuscript. All authors
926 discussed the results and commented on the manuscript.
927

928 **References**

929

930 1. Gokbuget D, Blelloch R. Epigenetic control of transcriptional regulation in
931 pluripotency and early differentiation. Development. 2019;146(19).
932 2. Kolodziejczyk AA, Kim JK, Tsang JC, Ilicic T, Henriksson J, Natarajan KN, et al.
933 Single Cell RNA-Sequencing of Pluripotent States Unlocks Modular Transcriptional
934 Variation. Cell Stem Cell. 2015;17(4):471-85.
935 3. Young RA. Control of the embryonic stem cell state. Cell. 2011;144(6):940-54.
936 4. Gabut M, Samavarchi-Tehrani P, Wang X, Slobodeniuc V, O'Hanlon D, Sung HK, et
937 al. An alternative splicing switch regulates embryonic stem cell pluripotency and
938 reprogramming. Cell. 2011;147(1):132-46.
939 5. Vissers C, Sinha A, Ming GL, Song H. The epitranscriptome in stem cell biology and
940 neural development. Neurobiol Dis. 2020;146:105139.
941 6. Yamazaki T, Liu L, Lazarev D, Al-Zain A, Fomin V, Yeung PL, et al. TCF3 alternative
942 splicing controlled by hnRNP H/F regulates E-cadherin expression and hESC
943 pluripotency. Genes Dev. 2018;32(17-18):1161-74.
944 7. Cruz-Molina S, Respuela P, Tebartz C, Kolovos P, Nikolic M, Fueyo R, et al. PRC2
945 Facilitates the Regulatory Topology Required for Poised Enhancer Function during
946 Pluripotent Stem Cell Differentiation. Cell Stem Cell. 2017;20(5):689-705 e9.
947 8. Lavarone E, Barbieri CM, Pasini D. Dissecting the role of H3K27 acetylation and
948 methylation in PRC2 mediated control of cellular identity. Nat Commun.
949 2019;10(1):1679.
950 9. Juan AH, Wang S, Ko KD, Zare H, Tsai PF, Feng X, et al. Roles of H3K27me2 and
951 H3K27me3 Examined during Fate Specification of Embryonic Stem Cells. Cell reports.
952 2016;17(5):1369-82.
953 10. de Sousa Abreu R, Penalva LO, Marcotte EM, Vogel C. Global signatures of protein
954 and mRNA expression levels. Mol Biosyst. 2009;5(12):1512-26.
955 11. Kristensen AR, Gsponer J, Foster LJ. Protein synthesis rate is the predominant
956 regulator of protein expression during differentiation. Mol Syst Biol. 2013;9:689.

bioRxiv preprint doi: https://doi.org/10.1101/2021.05.27.443845; this version posted May 29, 2021. The copyright holder for this preprint (which was not certified by peer review) is the author/funder. All rights reserved. No reuse allowed without permission.

957 12. Lu R, Markowetz F, Unwin RD, Leek JT, Airoldi EM, MacArthur BD, et al. Systems-
958 level dynamic analyses of fate change in murine embryonic stem cells. Nature.
959 2009;462(7271):358-62.
960 13. Maier T, Guell M, Serrano L. Correlation of mRNA and protein in complex
961 biological samples. FEBS Lett. 2009;583(24):3966-73.
962 14. Munoz J, Low TY, Kok YJ, Chin A, Frese CK, Ding V, et al. The quantitative
963 proteomes of human-induced pluripotent stem cells and embryonic stem cells. Mol Syst
964 Biol. 2011;7:550.
965 15. Schwanhausser B, Busse D, Li N, Dittmar G, Schuchhardt J, Wolf J, et al. Global
966 quantification of mammalian gene expression control. Nature. 2011;473(7347):337-42.
967 16. Gabut M, Bourdelais F, Durand S. Ribosome and Translational Control in Stem
968 Cells. Cells. 2020;9(2).
969 17. Sampath P, Pritchard DK, Pabon L, Reinecke H, Schwartz SM, Morris DR, et al. A
970 hierarchical network controls protein translation during murine embryonic stem cell
971 self-renewal and differentiation. Cell Stem Cell. 2008;2(5):448-60.
972 18. Signer RA, Magee JA, Salic A, Morrison SJ. Haematopoietic stem cells require a
973 highly regulated protein synthesis rate. Nature. 2014;509(7498):49-54.
974 19. Fortier S, MacRae T, Bilodeau M, Sargeant T, Sauvageau G. Haploinsufficiency
975 screen highlights two distinct groups of ribosomal protein genes essential for embryonic
976 stem cell fate. Proc Natl Acad Sci U S A. 2015;112(7):2127-32.
977 20. Bulut-Karslioglu A, Macrae TA, Oses-Prieto JA, Covarrubias S, Percharde M, Ku G,
978 et al. The Transcriptionally Permissive Chromatin State of Embryonic Stem Cells Is
979 Acutely Tuned to Translational Output. Cell Stem Cell. 2018;22(3):369-83 e8.
980 21. Corsini NS, Peer AM, Moeseneder P, Roiuk M, Burkard TR, Theussl HC, et al.
981 Coordinated Control of mRNA and rRNA Processing Controls Embryonic Stem Cell
982 Pluripotency and Differentiation. Cell Stem Cell. 2018;22(4):543-58 e12.
983 22. de la Cruz J, Gomez-Herreros F, Rodriguez-Galan O, Begley V, de la Cruz Munoz-
984 Centeno M, Chavez S. Feedback regulation of ribosome assembly. Curr Genet.
985 2018;64(2):393-404.
986 23. Klinge S, Woolford JL, Jr. Ribosome assembly coming into focus. Nature reviews
987 Molecular cell biology. 2019;20(2):116-31.
988 24. Pena C, Hurt E, Panse VG. Eukaryotic ribosome assembly, transport and quality
989 control. Nat Struct Mol Biol. 2017;24(9):689-99.
990 25. Woolnough JL, Atwood BL, Liu Z, Zhao R, Giles KE. The Regulation of rRNA Gene
991 Transcription during Directed Differentiation of Human Embryonic Stem Cells. PLoS
992 One. 2016;11(6):e0157276.
993 26. Eleuteri B, Aranda S, Ernfors P. NoRC Recruitment by H2A.X Deposition at rRNA
994 Gene Promoter Limits Embryonic Stem Cell Proliferation. Cell reports. 2018;23(6):1853-
995 66.
996 27. Kwon SC, Yi H, Eichelbaum K, Fohr S, Fischer B, You KT, et al. The RNA-binding
997 protein repertoire of embryonic stem cells. Nat Struct Mol Biol. 2013;20(9):1122-30.
998 28. Yang A, Shi G, Zhou C, Lu R, Li H, Sun L, et al. Nucleolin maintains embryonic stem
999 cell self-renewal by suppression of p53 protein-dependent pathway. J Biol Chem.
1000 2011;286(50):43370-82.
1001 29. Fong YW, Ho JJ, Inouye C, Tjian R. The dyskerin ribonucleoprotein complex as an
1002 OCT4/SOX2 coactivator in embryonic stem cells. Elife. 2014;3.
1003 30. Watanabe-Susaki K, Takada H, Enomoto K, Miwata K, Ishimine H, Intoh A, et al.
1004 Biosynthesis of ribosomal RNA in nucleoli regulates pluripotency and differentiation
1005 ability of pluripotent stem cells. Stem Cells. 2014;32(12):3099-111.

bioRxiv preprint doi: https://doi.org/10.1101/2021.05.27.443845; this version posted May 29, 2021. The copyright holder for this preprint (which was not certified by peer review) is the author/funder. All rights reserved. No reuse allowed without permission.

1006 31. You KT, Park J, Kim VN. Role of the small subunit processome in the maintenance
1007 of pluripotent stem cells. Genes Dev. 2015;29(19):2004-9.
1008 32. Gayraud-Morel B, Le Bouteiller M, Commere PH, Cohen-Tannoudji M, Tajbakhsh
1009 S. Notchless defines a stage-specific requirement for ribosome biogenesis during lineage
1010 progression in adult skeletal myogenesis. Development. 2018;145(23).
1011 33. Le Bouteiller M, Souilhol C, Beck-Cormier S, Stedman A, Burlen-Defranoux O,
1012 Vandormael-Pournin S, et al. Notchless-dependent ribosome synthesis is required for
1013 the maintenance of adult hematopoietic stem cells. J Exp Med. 2013;210(11):2351-69.
1014 34. Stedman A, Beck-Cormier S, Le Bouteiller M, Raveux A, Vandormael-Pournin S,
1015 Coqueran S, et al. Ribosome biogenesis dysfunction leads to p53-mediated apoptosis and
1016 goblet cell differentiation of mouse intestinal stem/progenitor cells. Cell Death Differ.
1017 2015;22(11):1865-76.
1018 35. Cormier S, Le Bras S, Souilhol C, Vandormael-Pournin S, Durand B, Babinet C, et
1019 al. The murine ortholog of notchless, a direct regulator of the notch pathway in
1020 Drosophila melanogaster, is essential for survival of inner cell mass cells. Mol Cell Biol.
1021 2006;26(9):3541-9.
1022 36. Han H, Irimia M, Ross PJ, Sung HK, Alipanahi B, David L, et al. MBNL proteins
1023 repress ES-cell-specific alternative splicing and reprogramming. Nature.
1024 2013;498(7453):241-5.
1025 37. Ozmadenci D, Feraud O, Markossian S, Kress E, Ducarouge B, Gibert B, et al.
1026 Netrin-1 regulates somatic cell reprogramming and pluripotency maintenance. Nat
1027 Commun. 2015;6:7398.
1028 38. Buganim Y, Faddah DA, Cheng AW, Itskovich E, Markoulaki S, Ganz K, et al. Single-
1029 cell expression analyses during cellular reprogramming reveal an early stochastic and a
1030 late hierarchic phase. Cell. 2012;150(6):1209-22.
1031 39. Chung KM, Kolling FWt, Gajdosik MD, Burger S, Russell AC, Nelson CE. Single cell
1032 analysis reveals the stochastic phase of reprogramming to pluripotency is an ordered
1033 probabilistic process. PLoS One. 2014;9(4):e95304.
1034 40. Guo L, Lin L, Wang X, Gao M, Cao S, Mai Y, et al. Resolving Cell Fate Decisions
1035 during Somatic Cell Reprogramming by Single-Cell RNA-Seq. Mol Cell. 2019;73(4):815-
1036 29 e7.
1037 41. Chen H, Aksoy I, Gonnot F, Osteil P, Aubry M, Hamela C, et al. Reinforcement of
1038 STAT3 activity reprogrammes human embryonic stem cells to naive-like pluripotency.
1039 Nat Commun. 2015;6:7095.
1040 42. Saveanu C, Namane A, Gleizes PE, Lebreton A, Rousselle JC, Noaillac-Depeyre J, et
1041 al. Sequential protein association with nascent 60S ribosomal particles. Mol Cell Biol.
1042 2003;23(13):4449-60.
1043 43. Sanghai ZA, Miller L, Molloy KR, Barandun J, Hunziker M, Chaker-Margot M, et al.
1044 Modular assembly of the nucleolar pre-60S ribosomal subunit. Nature.
1045 2018;556(7699):126-9.
1046 44. Wu S, Tutuncuoglu B, Yan K, Brown H, Zhang Y, Tan D, et al. Diverse roles of
1047 assembly factors revealed by structures of late nuclear pre-60S ribosomes. Nature.
1048 2016;534(7605):133-7.
1049 45. Zhou Y, Musalgaonkar S, Johnson AW, Taylor DW. Tightly-orchestrated
1050 rearrangements govern catalytic center assembly of the ribosome. Nat Commun.
1051 2019;10(1):958.
1052 46. Liang X, Zuo MQ, Zhang Y, Li N, Ma C, Dong MQ, et al. Structural snapshots of
1053 human pre-60S ribosomal particles before and after nuclear export. Nat Commun.
1054 2020;11(1):3542.

bioRxiv preprint doi: https://doi.org/10.1101/2021.05.27.443845; this version posted May 29, 2021. The copyright holder for this preprint (which was not certified by peer review) is the author/funder. All rights reserved. No reuse allowed without permission.

1055 47. Shubina MY, Arifulin EA, Sorokin DV, Sosina MA, Tikhomirova MA, Serebryakova
1056 MV, et al. The GAR domain integrates functions that are necessary for the proper
1057 localization of fibrillarin (FBL) inside eukaryotic cells. PeerJ. 2020;8:e9029.
1058 48. Weeks SE, Metge BJ, Samant RS. The nucleolus: a central response hub for the
1059 stressors that drive cancer progression. Cell Mol Life Sci. 2019;76(22):4511-24.
1060 49. De Los Angeles A, Ferrari F, Xi R, Fujiwara Y, Benvenisty N, Deng H, et al.
1061 Hallmarks of pluripotency. Nature. 2015;525(7570):469-78.
1062 50. Martello G, Smith A. The nature of embryonic stem cells. Annu Rev Cell Dev Biol.
1063 2014;30:647-75.
1064 51. Pinto JP, Kalathur RK, Oliveira DV, Barata T, Machado RS, Machado S, et al.
1065 StemChecker: a web-based tool to discover and explore stemness signatures in gene
1066 sets. Nucleic Acids Res. 2015;43(W1):W72-7.
1067 52. Oki S, Ohta T, Shioi G, Hatanaka H, Ogasawara O, Okuda Y, et al. ChIP-Atlas: a data-
1068 mining suite powered by full integration of public ChIP-seq data. EMBO Rep.
1069 2018;19(12).
1070 53. Stefkova K, Prochazkova J, Pachernik J. Alkaline phosphatase in stem cells. Stem
1071 Cells Int. 2015;2015:628368.
1072 54. Wobus AM, Guan K, Yang HT, Boheler KR. Embryonic stem cells as a model to
1073 study cardiac, skeletal muscle, and vascular smooth muscle cell differentiation. Methods
1074 Mol Biol. 2002;185:127-56.
1075 55. Frum T, Halbisen MA, Wang C, Amiri H, Robson P, Ralston A. Oct4 cell-
1076 autonomously promotes primitive endoderm development in the mouse blastocyst.
1077 Developmental cell. 2013;25(6):610-22.
1078 56. Funa NS, Schachter KA, Lerdrup M, Ekberg J, Hess K, Dietrich N, et al. beta-Catenin
1079 Regulates Primitive Streak Induction through Collaborative Interactions with
1080 SMAD2/SMAD3 and OCT4. Cell Stem Cell. 2015;16(6):639-52.
1081 57. Radzisheuskaya A, Chia Gle B, dos Santos RL, Theunissen TW, Castro LF, Nichols J,
1082 et al. A defined Oct4 level governs cell state transitions of pluripotency entry and
1083 differentiation into all embryonic lineages. Nature cell biology. 2013;15(6):579-90.
1084 58. Luhrig S, Siamishi I, Tesmer-Wolf M, Zechner U, Engel W, Nolte J. Lrrc34, a novel
1085 nucleolar protein, interacts with npm1 and ncl and has an impact on pluripotent stem
1086 cells. Stem Cells Dev. 2014;23(23):2862-74.
1087 59. Hernandez-Verdun D, Roussel P, Thiry M, Sirri V, Lafontaine DL. The nucleolus:
1088 structure/function relationship in RNA metabolism. Wiley interdisciplinary reviews
1089 RNA. 2010;1(3):415-31.
1090 60. Kater L, Thoms M, Barrio-Garcia C, Cheng J, Ismail S, Ahmed YL, et al. Visualizing
1091 the Assembly Pathway of Nucleolar Pre-60S Ribosomes. Cell. 2017;171(7):1599-610
1092 e14.
1093 61. Chaker-Margot M, Klinge S. Assembly and early maturation of large subunit
1094 precursors. RNA. 2019;25(4):465-71.
1095 62. Kappel L, Loibl M, Zisser G, Klein I, Fruhmann G, Gruber C, et al. Rlp24 activates
1096 the AAA-ATPase Drg1 to initiate cytoplasmic pre-60S maturation. The Journal of cell
1097 biology. 2012;199(5):771-82.
1098 63. Lo KY, Li Z, Bussiere C, Bresson S, Marcotte EM, Johnson AW. Defining the
1099 pathway of cytoplasmic maturation of the 60S ribosomal subunit. Mol Cell.
1100 2010;39(2):196-208.
1101 64. Pertschy B, Saveanu C, Zisser G, Lebreton A, Tengg M, Jacquier A, et al.
1102 Cytoplasmic recycling of 60S preribosomal factors depends on the AAA protein Drg1.
1103 Mol Cell Biol. 2007;27(19):6581-92.

bioRxiv preprint doi: https://doi.org/10.1101/2021.05.27.443845; this version posted May 29, 2021. The copyright holder for this preprint (which was not certified by peer review) is the author/funder. All rights reserved. No reuse allowed without permission.

1104 65. Tafforeau L, Zorbas C, Langhendries JL, Mullineux ST, Stamatopoulou V, Mullier R,
1105 et al. The complexity of human ribosome biogenesis revealed by systematic nucleolar
1106 screening of Pre-rRNA processing factors. Mol Cell. 2013;51(4):539-51.
1107 66. Talkish J, Zhang J, Jakovljevic J, Horsey EW, Woolford JL, Jr. Hierarchical
1108 recruitment into nascent ribosomes of assembly factors required for 27SB pre-rRNA
1109 processing in Saccharomyces cerevisiae. Nucleic Acids Res. 2012;40(17):8646-61.
1110 67. Weis F, Giudice E, Churcher M, Jin L, Hilcenko C, Wong CC, et al. Mechanism of
1111 eIF6 release from the nascent 60S ribosomal subunit. Nat Struct Mol Biol.
1112 2015;22(11):914-9.
1113 68. Gregory B, Rahman N, Bommakanti A, Shamsuzzaman M, Thapa M, Lescure A, et
1114 al. The small and large ribosomal subunits depend on each other for stability and
1115 accumulation. Life Sci Alliance. 2019;2(2).
1116 69. Rotenberg MO, Moritz M, Woolford JL, Jr. Depletion of Saccharomyces cerevisiae
1117 ribosomal protein L16 causes a decrease in 60S ribosomal subunits and formation of
1118 half-mer polyribosomes. Genes Dev. 1988;2(2):160-72.
1119 70. Zhao Y, Sohn JH, Warner JR. Autoregulation in the biosynthesis of ribosomes. Mol
1120 Cell Biol. 2003;23(2):699-707.
1121 71. Yi Y, Li Y, Meng Q, Li Q, Li F, Lu B, et al. A PRC2-independent function for EZH2 in
1122 regulating rRNA 2'-O methylation and IRES-dependent translation. Nature cell biology.
1123 2021;23(4):341-54.
1124 72. Mills EW, Green R. Ribosomopathies: There's strength in numbers. Science.
1125 2017;358(6363).
1126 73. Ingolia NT, Lareau LF, Weissman JS. Ribosome profiling of mouse embryonic stem
1127 cells reveals the complexity and dynamics of mammalian proteomes. Cell.
1128 2011;147(4):789-802.
1129 74. Friend K, Brooks HA, Propson NE, Thomson JA, Kimble J. Embryonic Stem Cell
1130 Growth Factors Regulate eIF2alpha Phosphorylation. PLoS One. 2015;10(9):e0139076.
1131 75. Carey BW, Markoulaki S, Beard C, Hanna J, Jaenisch R. Single-gene transgenic
1132 mouse strains for reprogramming adult somatic cells. Nat Methods. 2010;7(1):56-9.
1133 76. Doetschman TC, Eistetter H, Katz M, Schmidt W, Kemler R. The in vitro
1134 development of blastocyst-derived embryonic stem cell lines: formation of visceral yolk
1135 sac, blood islands and myocardium. J Embryol Exp Morphol. 1985;87:27-45.
1136 77. Robbins J, Doetschman T, Jones WK, Sanchez A. Embryonic stem cells as a model
1137 for cardiogenesis. Trends Cardiovasc Med. 1992;2(2):44-50.
1138 78. Moffat J, Grueneberg DA, Yang X, Kim SY, Kloepfer AM, Hinkle G, et al. A lentiviral
1139 RNAi library for human and mouse genes applied to an arrayed viral high-content
1140 screen. Cell. 2006;124(6):1283-98.
1141 79. Wee S, Wiederschain D, Maira SM, Loo A, Miller C, deBeaumont R, et al. PTEN-
1142 deficient cancers depend on PIK3CB. Proc Natl Acad Sci U S A. 2008;105(35):13057-62.
1143 80. Wiederschain D, Wee S, Chen L, Loo A, Yang G, Huang A, et al. Single-vector
1144 inducible lentiviral RNAi system for oncology target validation. Cell cycle.
1145 2009;8(3):498-504.
1146 81. Rueden CT, Schindelin J, Hiner MC, DeZonia BE, Walter AE, Arena ET, et al.
1147 ImageJ2: ImageJ for the next generation of scientific image data. BMC Bioinformatics.
1148 2017;18(1):529.
1149 82. Madeira F, Park YM, Lee J, Buso N, Gur T, Madhusoodanan N, et al. The EMBL-EBI
1150 search and sequence analysis tools APIs in 2019. Nucleic Acids Res.
1151 2019;47(W1):W636-W41.

bioRxiv preprint doi: https://doi.org/10.1101/2021.05.27.443845; this version posted May 29, 2021. The copyright holder for this preprint (which was not certified by peer review) is the author/funder. All rights reserved. No reuse allowed without permission.

1152 83. Waterhouse AM, Procter JB, Martin DM, Clamp M, Barton GJ. Jalview Version 2--a
1153 multiple sequence alignment editor and analysis workbench. Bioinformatics.
1154 2009;25(9):1189-91.
1155 84. Bertoni M, Kiefer F, Biasini M, Bordoli L, Schwede T. Modeling protein quaternary
1156 structure of homo- and hetero-oligomers beyond binary interactions by homology.
1157 Scientific reports. 2017;7(1):10480.
1158 85. Bienert S, Waterhouse A, de Beer TA, Tauriello G, Studer G, Bordoli L, et al. The
1159 SWISS-MODEL Repository-new features and functionality. Nucleic Acids Res.
1160 2017;45(D1):D313-D9.
1161 86. Guex N, Peitsch MC, Schwede T. Automated comparative protein structure
1162 modeling with SWISS-MODEL and Swiss-PdbViewer: a historical perspective.
1163 Electrophoresis. 2009;30 Suppl 1:S162-73.
1164 87. Waterhouse A, Bertoni M, Bienert S, Studer G, Tauriello G, Gumienny R, et al.
1165 SWISS-MODEL: homology modelling of protein structures and complexes. Nucleic Acids
1166 Res. 2018;46(W1):W296-W303.
1167 88. Wang L, Wang S, Li W. RSeQC: quality control of RNA-seq experiments.
1168 Bioinformatics. 2012;28(16):2184-5.
1169 89. Soneson C, Love MI, Robinson MD. Differential analyses for RNA-seq: transcript-
1170 level estimates improve gene-level inferences. F1000Res. 2015;4:1521.
1171 90. Love MI, Huber W, Anders S. Moderated estimation of fold change and dispersion
1172 for RNA-seq data with DESeq2. Genome Biol. 2014;15(12):550.
1173 91. Maere S, Heymans K, Kuiper M. BiNGO: a Cytoscape plugin to assess
1174 overrepresentation of gene ontology categories in biological networks. Bioinformatics.
1175 2005;21(16):3448-9.
1176 92. Shannon P, Markiel A, Ozier O, Baliga NS, Wang JT, Ramage D, et al. Cytoscape: a
1177 software environment for integrated models of biomolecular interaction networks.
1178 Genome Res. 2003;13(11):2498-504.
1179

1180

bioRxiv preprint doi: https://doi.org/10.1101/2021.05.27.443845; this version posted May 29, 2021. The copyright holder for this preprint (which was not certified by peer review) is the author/funder. All rights reserved. No reuse allowed without permission.

1181 **Figure 1. Rsl24d1 expression is enriched in PSCs.**

1182 (A) Box plot representation of mRNA expression changes in mouse PSCs (5 ESC lines
1183 and 2 iPSC clones) and 6 differentiated cell lines, measured by RNA-seq, for 4 functional
1184 gene categories: factors involved in common biogenesis steps (Biogenesis), specific
1185 biogenesis factors of the 40S (SSU biog.) or of the 60S subunits (LSU biog.), and
1186 ribosomal proteins (RP). Outlier values are represented by individual grey circles and
1187 Rsl24d1 is indicated by a black circle. Additional details are provided in Figure S1A and
1188 individual data are available in Table S1.

1189 (B) Representative western blot analyses of RSL24D1 (n=6), POU5F1 (n=4) and RPL8
1190 (n=5) in mouse CGR8 ESCs cultivated in ground state (ESC^{2i}) or naive (ESC^{FBS})
1191 conditions or differentiated in embryoid bodies (EB) for 12 days (EB^{12}). Lanes 1 to 3
1192 correspond to serial of dilutions of ESC^{FBS} (1:1, 1:3 and 1:9, respectively). Tri-Chloro-
1193 Ethanol (TCE) labeling of tryptophan-containing proteins (referred to as Total Proteins)
1194 is used for normalization. Quantifications of RSL24D1 and RPL8 signals normalized to
1195 total proteins and relative to the ESC^{2i} condition (Rel. exp. (%)) are indicated below each
1196 corresponding panels. Indicated P values are relative to ESC^{FBS} conditions (paired two-
1197 tailed Student's t-test): *** pval<0.001, N.S.: not significant (pval>0.05).

1198 (C) Representative western blots of RSL24D1 and POU5F1 in 3 unrelated mouse ESC
1199 lines (CGR8, R1 and G4) cultivated in ESC^{2i}, ESC^{FBS} and differentiated (EB^{12}) conditions,
1200 as in panel B. β-TUBULIN levels are shown as a loading control.

1201 (D) Representative western blot analyses of RSL24D1 (n=6), POU5F1 (n=4) and RPL8
1202 (n=4) in MEFs and in iPSCs reprogrammed from MEFs derived from doxycycline-
1203 inducible Col1a1-tetO-OKMS mice after ectopic induction of Pou5f1, Sox2, Klf4 and cMyc
1204 expression. TCE labeling of tryptophan-containing proteins (referred as Total Proteins)
1205 is used for normalization. Quantifications of RSL24D1 and RPL8 signals normalized to

bioRxiv preprint doi: https://doi.org/10.1101/2021.05.27.443845; this version posted May 29, 2021. The copyright holder for this preprint (which was not certified by peer review) is the author/funder. All rights reserved. No reuse allowed without permission.

1206 total protein and relative to the "MEF" conditions (Rel. exp. (%)) are indicated below
1207 each corresponding panels. Indicated P values are relative to "MEF" conditions (paired
1208 two-tailed Student's t-test): ** pval<0.005, N.S.: not significant (pval>0.05).
1209 (E) Box plot representation of normalized RSL24D1 mRNA expression levels in RPKMs
1210 (Reads per kilo base per million mapped reads) across 5 human PSC models, 7 human
1211 cell lines and 16 adult tissues based on published RNA-seq profiles (36). P values are
1212 indicated and are relative to human PSCs (unpaired two-tailed Student's t-test): *
1213 pval<0,05.
1214 (F) Representative western blots of RSL24D1 in human OSCAR ESCs maintained in
1215 pluripotent state in the presence of FGF2 or *in vitro* differentiated into EBs (Diff.). TCE
1216 labeling of proteins ("Total Proteins") is used as a loading control.
1217
1218 **Figure 2. RSL24D1 protein is associated with pre-60S subunits in mouse ESCs.**
1219 (A) Comparison of the mouse RSL24D1 predicted structure (amino acids 1-135, red
1220 colour) with the yeast Rlp24 structure (amino acids 1-149, PDB 6N8J grey colour, left
1221 panel) and the human RSL24D1 structure (amino acids 1-163, PDB 6LSS, blue colour,
1222 right panel) (45-46). The mouse RSL24D1 protein structure was predicted from the
1223 6N8J and 6LSS structures using the swiss-model structure assessment tool (87).
1224 (B) Representative images of naive CGR8 cells stained with Hoechst and with anti-FBL
1225 and anti-RSL24D1 antibodies (20X objective).
1226 (C) Nucleo-cytoplasmic fractionations ("total") followed by sucrose cushion
1227 purifications of nuclear pre-ribosomes ("pre-rib.") and cytoplasmic ribosomes
1228 ("ribosomes") from CGR8 ESC^{FBS}. Representative western blot analysis of RSL24D1,
1229 RPL24 and RPL8 (LSU), RPS6 (SSU) and EIF6 (RBF). HISTONE H3 and GAPDH are shown
1230 as specific nuclear and cytoplasmic proteins, respectively.

bioRxiv preprint doi: https://doi.org/10.1101/2021.05.27.443845; this version posted May 29, 2021. The copyright holder for this preprint (which was not certified by peer review) is the author/funder. All rights reserved. No reuse allowed without permission.

1231 (D) Polysome profiling by centrifugation on sucrose gradient of CGR8 ESC^{FBS}
1232 cytoplasmic extracts. Ribosome-free fractions (free mRNPs), 40S, 60S, 80S monosomes
1233 and polysomes are detected by UV-absorbance and indicated on the absorbance curve
1234 (upper panel). Representative western blots of gradient fractions using antibodies
1235 targeting RSL24D1, EIF6 (LSU), RPL8 (LSU) and RPS6 (SSU) (lower panel). GAPDH is
1236 used as a control of the free mRNPs. The fractions are indicated below the GAPDH panel.
1237

1238 **Figure 3. RSL24D1 depletion alters ribosome biogenesis and protein translation.**

1239 (A) Representative immunoblot of RSL24D1 in total extracts from si-CTL and si-Rsl24d1
1240 treated CGR8 ESC^{FBS}. Lanes 1 to 3 correspond to serial dilutions of ESC^{FBS} (1:1, 1:3 and
1241 1:9, respectively). TCE labeling of tryptophan-containing proteins (referred as Total
1242 Proteins) is used for normalization. Quantifications of RSL24D1 signals normalized to
1243 total proteins and relative to the si-CTL-treated conditions (Rel. exp. (%)) are indicated
1244 below each panel. The indicated P value is relative to the si-CTL-treated conditions
1245 (unpaired two-tailed Student's t test): **** pval<0.0001.
1246 (B) Polysome profiling by centrifugation on sucrose gradient of cytoplasmic extracts
1247 from naive CGR8 cells treated with non-targeting siRNAs (grey color) or siRNAs
1248 targeting Rsl24d1 (black color). 40S, 60S, 80S monosome and polysomes are detected
1249 by UV-absorbance and indicated on the absorbance curve.
1250 (C) Histograms indicating ratios of 60S/40S and 80S/40S absorbance peaks calculated
1251 by determining the area under the curve (AUC) for the 40S, 60S and 80S absorbance
1252 signals (n=3). P values are indicated (unpaired two-tailed Student's t test): * (pval<0.05).
1253 (D) Nucleo-cytoplasmic fractionation followed by ribosome purifications on sucrose
1254 cushions ("pre-rib." and "ribosomes") of CGR8 ESC^{FBS} transfected with non-targeting (si-
1255 CTL) or Rsl24d1-targeting siRNAs. Nuclear and cytoplasmic extracts are both indicated

bioRxiv preprint doi: https://doi.org/10.1101/2021.05.27.443845; this version posted May 29, 2021. The copyright holder for this preprint (which was not certified by peer review) is the author/funder. All rights reserved. No reuse allowed without permission.

1256 by "Total". Western blots are probed with anti-RSL24D1, -RPL24, -RPL8 and -EIF6
1257 antibodies. Immunoblots for HISTONE H3 and GAPDH are shown as specific nuclear and
1258 cytoplasmic proteins, respectively.
1259 (E) Representative immunoblots of RSL24D1, RPL24 and EIF6 (n=3) in total extracts
1260 from si-CTL and si-Rsl24d1 treated CGR8 ESC^{FBS}. Lanes 1 to 3 correspond to serial
1261 dilutions of si-CTL-treated ESC^{FBS} (1:1, 1:3 and 1:9, respectively). TCE labeling of
1262 tryptophan-containing proteins (referred as Total Proteins) is used for normalization.
1263 Quantifications of the RPL24, EIF6 and RSL24D1 signals normalized to total proteins
1264 and relative to the si-CTL-treated condition (Rel. exp. (%)) are indicated below each
1265 panel. The indicated P values are relative to the si-CTL-treated conditions (unpaired
1266 two-tailed Student's t test): **** pval<0.0001, ** pval<0.01, * pval<0.05.
1267 (F) Representative autoradiography (upper panel) and coomassie staining (lower panel)
1268 of SDS-PAGE of total extracts from si-CTL and si-Rsl24d1 treated CGR8 ESC^{FBS}, in the
1269 presence or absence of Cycloheximide (CHX) and ^{35}S-labelled methionine and cysteine.
1270 Quantifications of ^{35}S signals (autoradiography) are normalized to total proteins
1271 (coomassie staining) and expressed relative to si-CTL- and ^{35}S-methionine-treated
1272 ESC^{FBS} (n=3). Indicated P values are calculated relative to si-CTL-treated conditions
1273 (unpaired two-tailed Student's t test): ** pval<0.01, N.S.: pval>0.05.
1274

1275 **Figure 4. RSL24D1 is required to maintain the regulation of pluripotency and**
1276 **differentiation transcriptional programs.**

1277 (A) Gene ontology enrichment analysis of biological process terms for genes displaying
1278 significant expression changes by RNA-seq analysis in CGR8 cells treated with Rsl24d1
1279 siRNAs. The left and right panels represent hierarchical trees of the most enriched terms
1280 in genes up- or downregulated in Rsl24d1-depleted cells, respectively. The size of the

bioRxiv preprint doi: https://doi.org/10.1101/2021.05.27.443845; this version posted May 29, 2021. The copyright holder for this preprint (which was not certified by peer review) is the author/funder. All rights reserved. No reuse allowed without permission.

1281 nodes represents the numbers of genes associated to each GO term, and the
1282 corresponding p-values are indicated by colour codes, according to the scale provided.
1283 The most represented GO term categories are indicated. The corresponding data are
1284 available in Table S3.
1285 (B) Radar plot summarizing the Stemchecker analysis for PTFs and chromatin-
1286 associated factors with a significant association score to the 250 upregulated and the
1287 259 downregulated genes in Rsl24d1-depleted ESC^{FBS} CGR8 cells. The corresponding
1288 data are available in Table S4.
1289 (C) Diagram showing the relative proportion of up- and downregulated genes in
1290 Rsl24d1-depleted naive CGR8 cells that contain binding sites in their promoter region
1291 (+/- 1kb from transcription start sites) for indicated transcription and chromatin-
1292 associated factors, established by ChIP-seq analyses (52). P values are indicated (Fisher
1293 exact test): * pval<0.05, **** pval<0.0001, N.S.: not significant (pval>0.05).
1294 (D) Analysis of the proportion of genes displaying similar expression changes, either up-
1295 or downregulation, in Rsl24d1-depleted CGR8 cells and in EED$^{-/-}$ or EZH2$^{-/-}$ ESCs (7-8).
1296

1297 **Figure 5. RSL24D1 depletion impairs the translation of core PRC2 factors and the**
1298 **expression of key PTFs.**
1299 (A) Relative proportions of Eed, Ezh2 and Suz12 mRNAs detected by qRT-PCR in free
1300 mRNP, monosomal or polysomal fractions, based on quantifications detailed in the
1301 supplemental Figure S5C, in CGR8 ESC^{FBS} treated with CTL- (grey) or Rsl24d1-targeting
1302 siRNAs (black) (n=3). P values are indicated (paired two-tailed Student's t-test): **
1303 pval<0.005, * pval<0.05, N.S.: not significant (pval>0.05).
1304 (B) Representative immunoblots of RSL24D1 (n=3) and 3 PCR2 proteins (EED n=3,
1305 EZH2 n=3, SUZ12 n=4) in CGR8 ESC^{FBS} treated with non-targeting or Rsl24d1-targeting

bioRxiv preprint doi: https://doi.org/10.1101/2021.05.27.443845; this version posted May 29, 2021. The copyright holder for this preprint (which was not certified by peer review) is the author/funder. All rights reserved. No reuse allowed without permission.

1306 siRNAs. Lanes 1 to 3 correspond to serial dilutions of si-CTL-treated ESC^{FBS} (1:1, 1:3 and
1307 1:9, respectively). TCE labeling of tryptophan-containing proteins (referred as Total
1308 Proteins) is used for normalization. Quantifications of RSL24D1, EED, EZH2 and SUZ12
1309 signals normalized to total proteins and relative to the si-CTL-treated conditions (Rel.
1310 exp. (%)) are indicated below each panel. P values are indicated and relative to the si-
1311 CTL-treated conditions (paired two-tailed Student's t-test): ** pval<0.01, * pval<0.05,
1312 N.S.: not significant (pval>0.05).
1313 (C) As previously described for panel B for POU5F1 (n=3) and NANOG (n=3) in CGR8
1314 cells treated with non-targeting (si-CTL) or Rsl24d1-targeting siRNAs. * pval<0.05.
1315
1316 **Figure 6. RSL24D1 is required for mouse ESC proliferation and self-renewal.**
1317 (A) Analysis of proliferative capacities defined by the cell growth index quantified by the
1318 xCELLigence RTCA technology in the first 12 hours after plating CGR8 cells in ESC^{FBS}
1319 conditions. Cells were infected with lentiviral vectors expressing a control non-targeting
1320 shRNA (grey dots, sh-Control, n=14 wells), or 2 distinct shRNAs targeting Rsl24d1
1321 (black dots, sh-Rsl24d1-1, n=15 wells; sh-Rsl24d1-2, n=16 wells). P values are indicated
1322 and relative to the sh-control condition (unpaired two-tailed Student's t test): **
1323 pval<0.005, **** pval<0.0001.
1324 (B) Long term proliferation estimated by cell confluency analysis of naive CGR8 cells
1325 expressing a non-targeting shRNA (sh-Control, grey squares) or 2 distinct shRNAs
1326 targeting Rsl24d1 (sh-Rsl24d1-1, black triangles and sh-Rsl24d1-2, white circles)(n=6).
1327 (C) Analysis of the self-renewing capacities of CGR8 cells in ESC^{FBS} conditions estimated
1328 by the quantification of individual colonies with alkaline phosphatase activity detected
1329 by colorimetric labelling (corresponding raw data are detailed in Supplemental Fig. 6C).
1330 CGR8 colonies expressing control- (n=4 wells), Pou5f1- (n=4 wells) or Rsl24d1-targeting

bioRxiv preprint doi: https://doi.org/10.1101/2021.05.27.443845; this version posted May 29, 2021. The copyright holder for this preprint (which was not certified by peer review) is the author/funder. All rights reserved. No reuse allowed without permission.

1331 shRNAs (sh-Rsl24d1-1, sh-Rsl24d1-2) (n=5 wells) were compared. * pval<0.05,
1332 unpaired two-tailed Student's t test.
1333 (D) Analysis of *in vitro* differentiation capacities of CGR8 cells expressing control- (n=7
1334 wells), Pou5f1- (n=5 wells) or Rsl24d1-shRNAs (n=7 wells) defined by the proportion of
1335 seeded embryoid bodies surviving and growing during a 12-day differentiation course.
1336 **** pval<0.0001, N.S.: not significant (pval>0.05), unpaired two-tailed Student's t test.
1337 (E) Analysis of the proportion of 12-day old EBs, generated from CGR8 cells expressing
1338 control- (n=7 wells), Pou5f1- (n=5 wells) or Rsl24d1-shRNAs (n=7 wells), containing
1339 functional self-beating cardiomyocytes. *** pval<0.001, * pval<0.05, N.S.: not significant
1340 (pval>0.05), unpaired two-tailed Student's t test.
1341
1342 **Figure 7. Model describing the functions of RSL24D1 in the LSU biogenesis and in**
1343 **the translational regulation of key pluripotency and developmental programs in**
1344 **mouse ESCs.**
1345

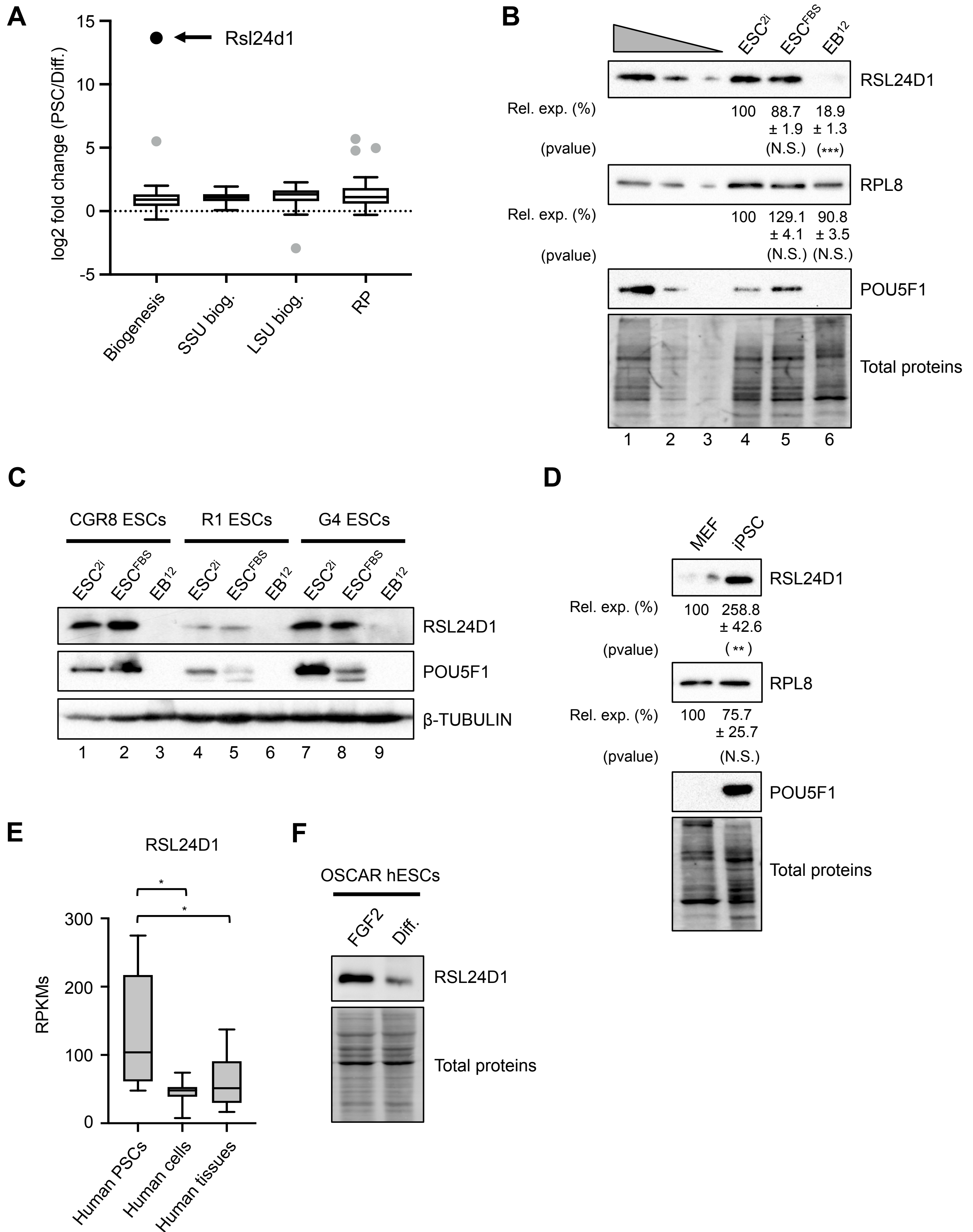
A
log2 fold change (PSC/Diff.)
15
10
5
0
-5
Rsl24d1
Biogenesis
SSU biog.
LSU biog.
RP
B
ESC2i
ESCFBS
EB12
RSL24D1
Rel. exp. (%)
100
88.7 ± 1.9
18.9 ± 1.3
(pvalue)
(N.S.)
(***)
RPL8
Rel. exp. (%)
100
129.1 ± 4.1
90.8 ± 3.5
(pvalue)
(N.S.)
(N.S.)
POU5F1
Total proteins
1 2 3 4 5 6
C
CGR8 ESCs
R1 ESCs
G4 ESCs
ESC2i ESCFBS EB12
RSL24D1
POU5F1
β-TUBULIN
1 2 3 4 5 6 7 8 9
D
MEF
iPSC
RSL24D1
Rel. exp. (%)
100
258.8 ± 42.6
(pvalue)
(**)
RPL8
Rel. exp. (%)
100
75.7 ± 25.7
(pvalue)
(N.S.)
POU5F1
Total proteins
E
RSL24D1
RPKMs
300
200
100
0
*
*
Human PSCs
Human cells
Human tissues
F
OSCAR hESCs
FGF2
Diff.
RSL24D1
Total proteins

bioRxiv preprint doi: https://doi.org/10.1101/2021.05.27.443845; this version posted May 29, 2021. The copyright holder for this preprint (which was not certified by peer review) is the author/funder. All rights reserved. No reuse allowed without permission.

A

Yeast Rlp24: aa 1-149
Mouse RSL24D1: aa 1-135

Human RSL24D1: aa 1-163
Mouse RSL24D1: aa 1-135

B

RSL24D1
FBL
Hoechst
overlay

C

nucleus
cytoplasm
total
pre-rib.
total
ribosomes
RSL24D1
RPL24
RPL8
RPS6
EIF6
HISTONE 3
GAPDH

D

UV absorbance (arbitrary unit)
80
70
60
50
40
30
20
10
0
free mRNPs
40S
60S
80S
Polysomes
10%
50%
sucrose gradient

40S
60S
80S
Polysomes
RSL24D1
EIF6
RPL8
RPS6
GAPDH
1 2 3 4 5 6 7 8 9 10 11 12 13 14

Figure 3, Durand et al.

A

si-CTL si-Rsl24d1

RSL24D1

Rel. exp. (%) 100 32.9 ± 3.7

(pvalue) (****)

Total proteins

1 2 3 4 5

B

si-CTL

si-Rsl24d1

40S 60S 80S

Polysomes

UV absorbance (arbitrary unit)

100 80 60 40 20 0

10% sucrose gradient 50%

C

si-CTL

si-Rsl24d1

Ratios of AUC

2.0 1.5 1.0 0.5 0

60S/40S 80S/40S

D

Nucleus Cytoplasm

Total pre-rib. Total ribosomes

si-CTL

si-Rsl24d1

RSL24D1

RPL24

EIF6

RPL8

GAPDH

Histone H3

1 2 3 4 5 6 7 8

E

si-CTL si-Rsl24d1

RPL24

Rel. exp. (%) 100 42.3 ± 5.9

(pvalue) (**)

EIF6

Rel. exp. (%) 100 81.6 ± 3.5

(pvalue) (*)

RSL24D1

Rel. exp. (%) 100 35.5 ± 3.9

(pvalue) (****)

Total proteins

1 2 3 4 5

F

no ^{35}S | ^{35}S + CHX | ^{35}S

si-CTL

si-Rsl24d1

180 KDa

10 KDa

Autoradio-graphy

Relative *de novo* protein synthesis (%) 10.9 ± 2.5 9.1 ± 3.6 100 56.7 ± 14.4

(pvalue) (N.S.) (**)

180 KDa

10 KDa

Total protein

1 2 3 4 5 6

Figure 4, Durand et al.

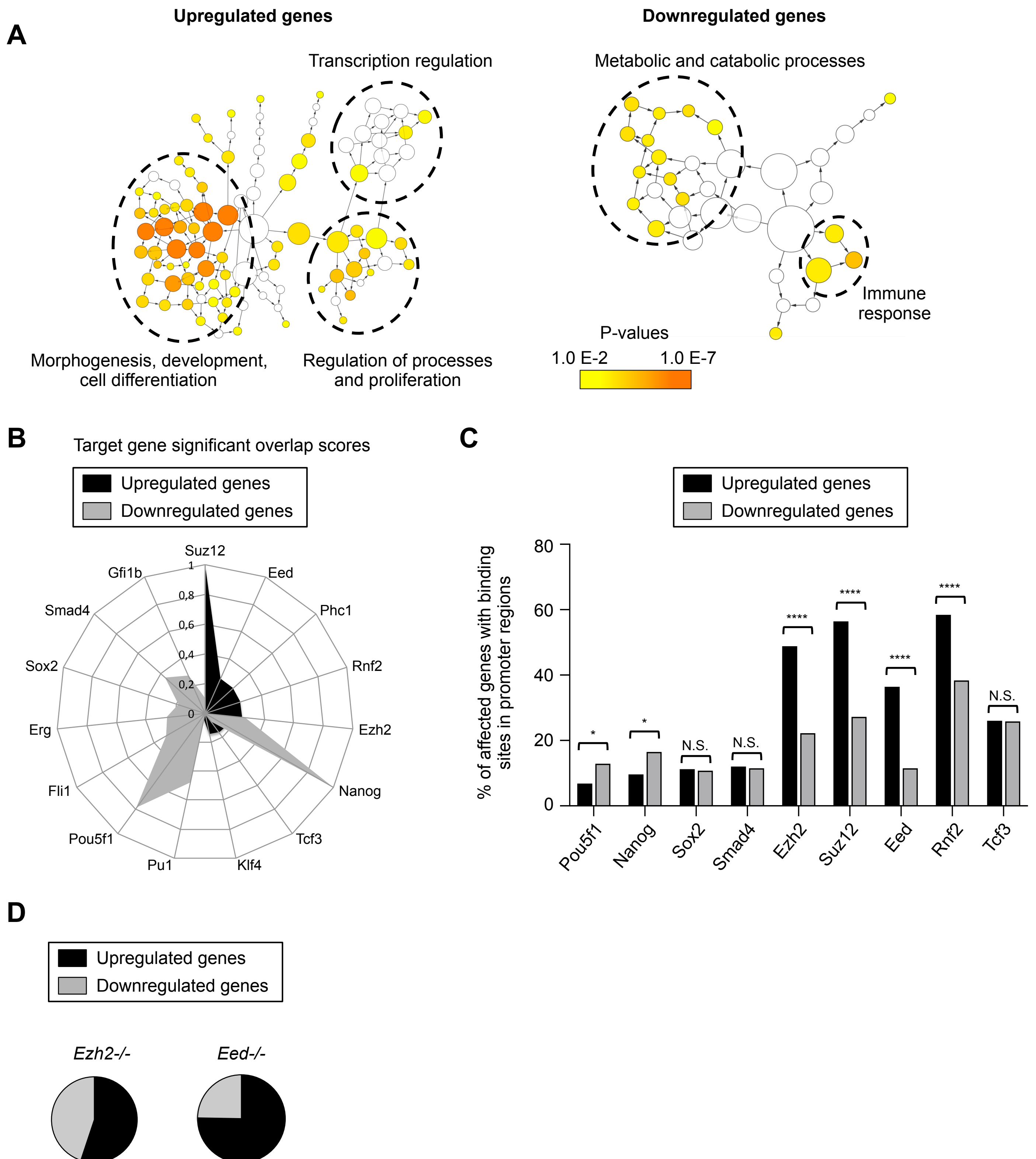

Figure 5, Durand et al.

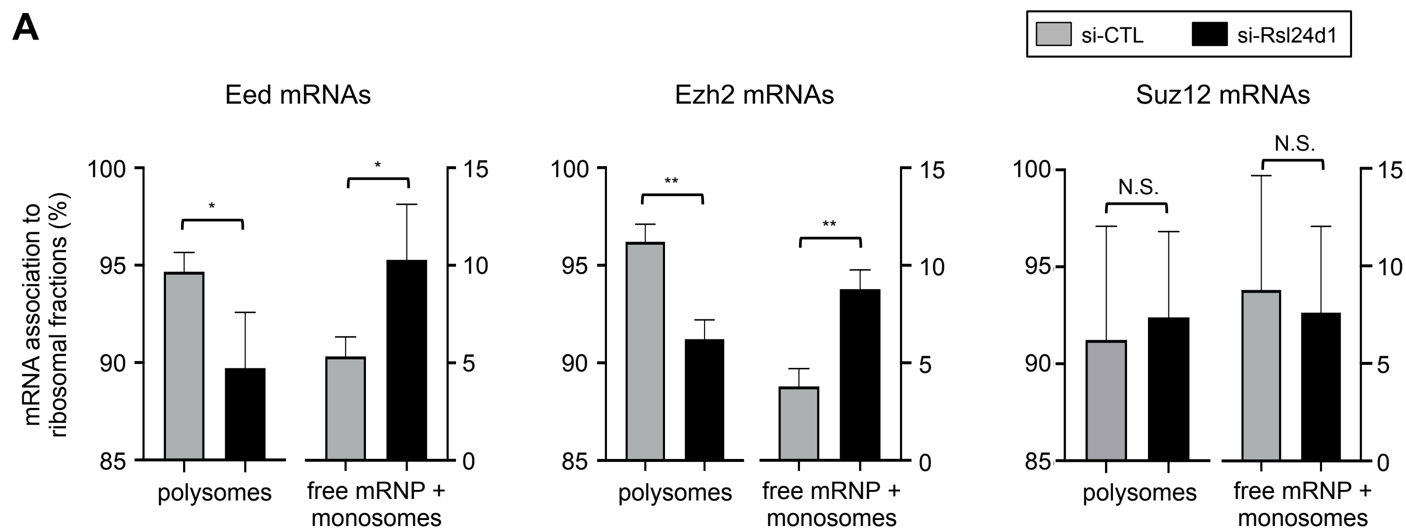

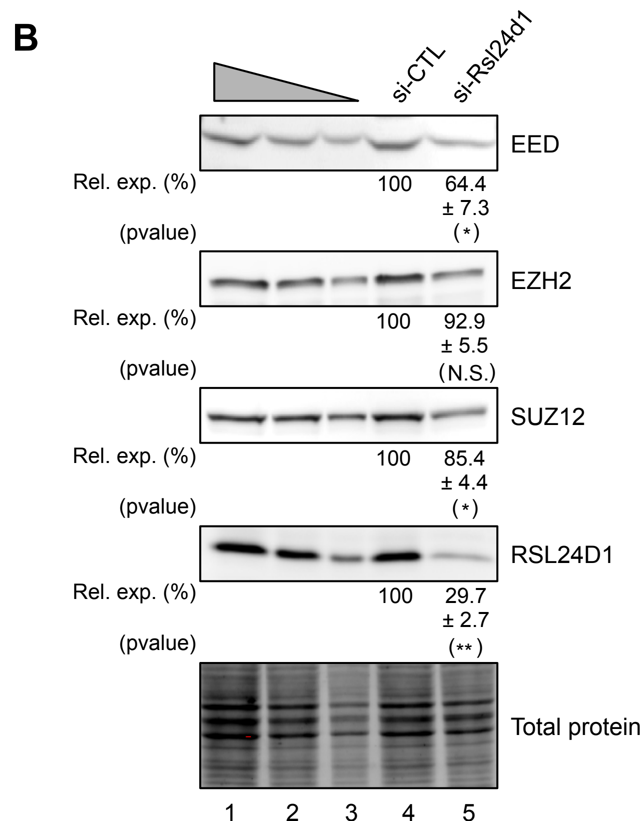

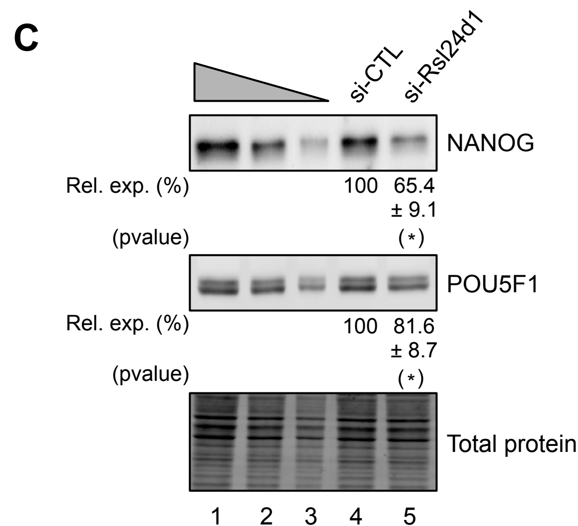

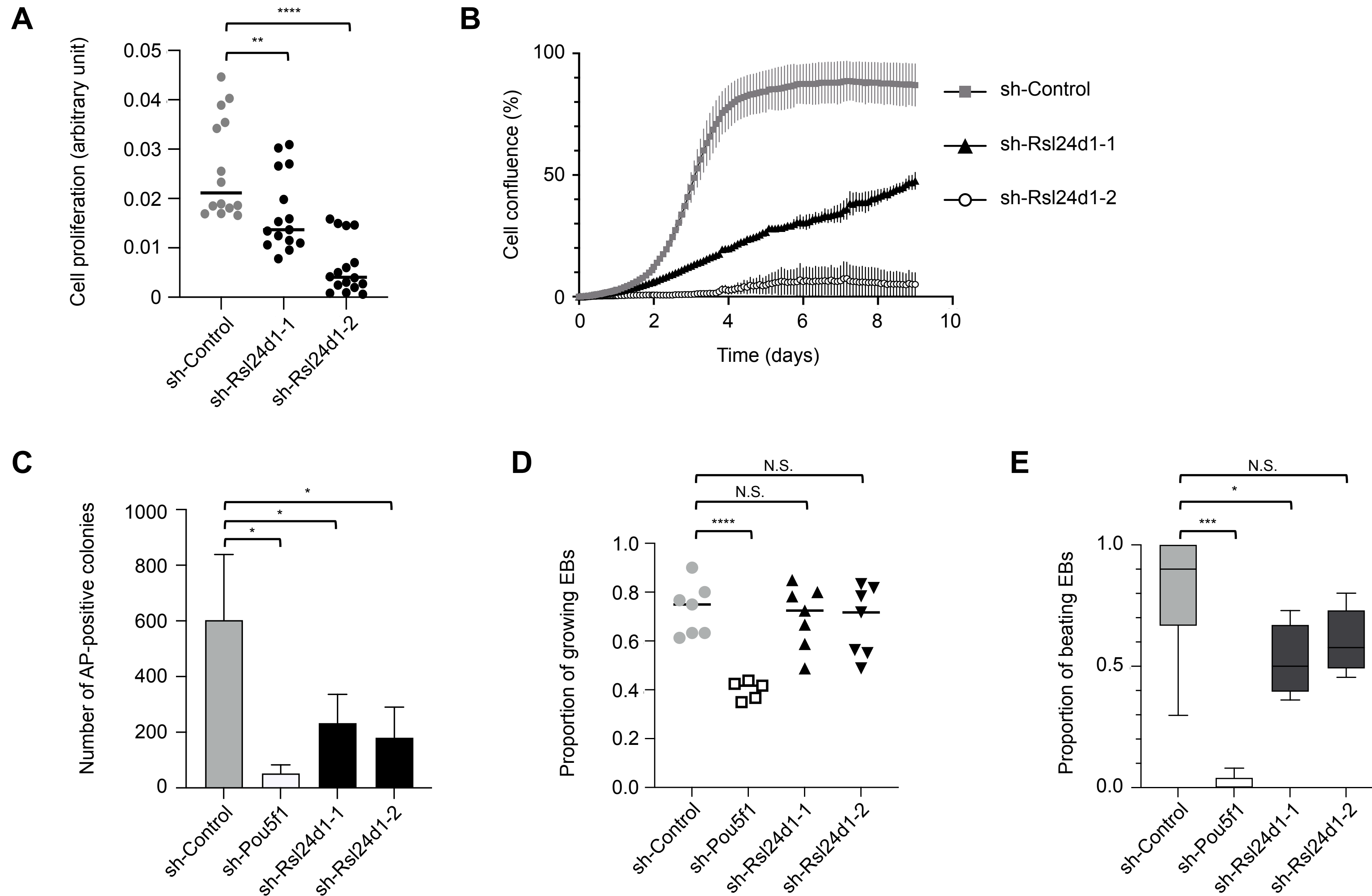
A
B
C
D
E
Cell proliferation (arbitrary unit)
0.05
0.04
0.03
0.02
0.01
0
****
**
sh-Control
sh-Rsl24d1-1
sh-Rsl24d1-2
Cell confluence (%)
100
50
0
0
2
4
6
8
10
Time (days)
sh-Control
sh-Rsl24d1-1
sh-Rsl24d1-2
Number of AP-positive colonies
1000
800
600
400
200
0
*
*
*
sh-Control
sh-Pou5f1
sh-Rsl24d1-1
sh-Rsl24d1-2
Proportion of growing EBs
1.0
0.8
0.6
0.4
0.2
0.0
N.S.
N.S.
****
sh-Control
sh-Pou5f1
sh-Rsl24d1-1
sh-Rsl24d1-2
Proportion of beating EBs
1.0
0.5
0.0
N.S.
*
***
sh-Control
sh-Pou5f1
sh-Rsl24d1-1
sh-Rsl24d1-2

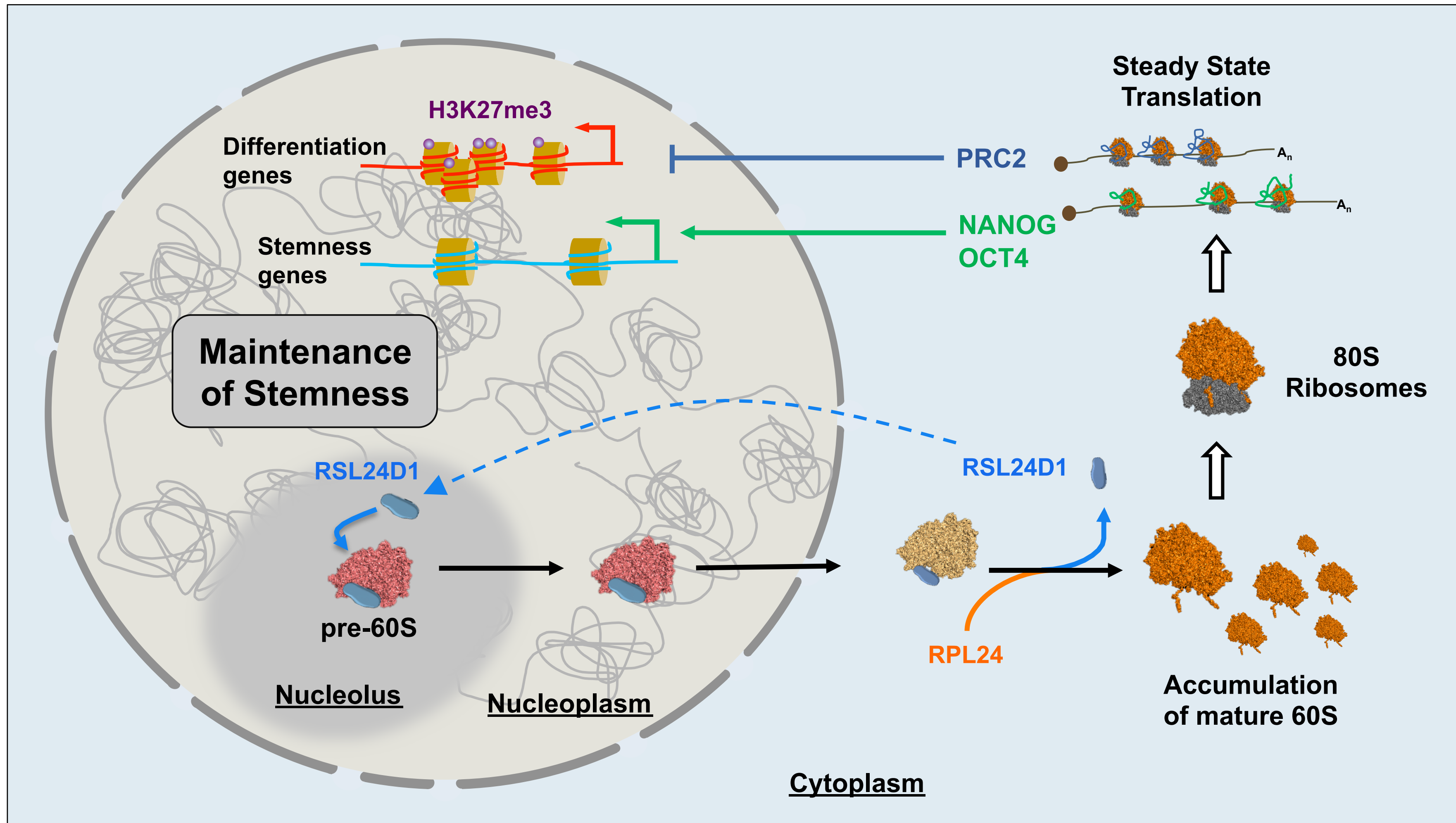
H3K27me3
Differentiation genes
Stemness genes
Maintenance of Stemness
RSL24D1
pre-60S
Nucleolus
Nucleoplasm
Steady State Translation
PRC2
NANOG
OCT4
80S Ribosomes
RSL24D1
RPL24
Accumulation of mature 60S
Cytoplasm